

## An analysis of a relatively rare case of continental blocking

By ANTHONY R. LUPO\* and LANCE F. BOSART

*The University at Albany, USA*

(Received 10 March 1997; revised 27 April 1998)

### SUMMARY

Planetary- and synoptic-scale analyses of a relatively rare continental blocking event that occurred over North America during the spring of 1980 are undertaken to determine whether or not this event was different from its counterparts which occur over oceanic regions. The planetary-scale analysis demonstrates that during the spring season a ridge was located further inland over the North American continent and amplified with respect to climatology. The position of this ridge may have been linked to a broad region of colder-than-normal sea surface temperatures found over the north central Pacific during the spring season and much of the previous winter. Simple ‘Sutcliffe-type’ and thermodynamic analyses of the accompanying lower-tropospheric warm anomaly associated with the ridging show that lower-tropospheric temperature advection and subsidence associated with anticyclonic-vorticity advection by the time-mean thermal wind produced much of the anomalous warmth.

A simple synoptic-scale analysis was performed using both the Zwack–Okossi (ZO) equation and potential vorticity (PV) thinking approaches. These complementary analyses demonstrated that synoptic-scale cyclones were instrumental in the formation and maintenance (and/or intensification) of this blocking event. The PV analysis demonstrated that low-PV air was swept polewards and then was advected over the blocking region sustaining the broad region of low potential vorticity associated with the block over North America. The ZO analysis showed that the advection of anticyclonic vorticity was the most important mechanism forcing geopotential-height rises at 500 hPa over the block centre. The region of low PV and ZO height rises could be associated with the anticyclonic-shear side of an upstream jet maximum typically found in association with developing and/or intensifying blocking events. Thus, negative PV advection correlated significantly with calculated ZO height rises. Finally, it is suggested that a favourable phase relationship between the upstream cyclones and the large-scale ridge is necessary for block development or intensification.

KEYWORDS: Atmospheric dynamics North America Potential vorticity Synoptic analysis

### 1. INTRODUCTION

In recent years, substantial progress has been made in understanding both the climatological behaviour of blocking anticyclones (e.g. Rex 1950; Triedl *et al.* 1981; Lejenas and Okland 1983; Shukla and Mo 1983; Lupo and Smith 1995a, hereafter LS95a) and the atmospheric dynamics associated with the formation and maintenance of them (e.g. Tung and Lindzen 1979a, b; McWilliams 1980; Kalnay-Rivas and Merkin 1981; Frederiksen 1982, 1983; Shutts 1983, 1986; Colucci 1985, 1987; Mullen 1986, 1987; Tsou and Smith 1990; Alberta *et al.* 1991; Lupo and Smith 1995b, hereafter LS95b). Despite this progress, forecasting the formation and maintenance of blocking anticyclones remains a difficult problem (e.g. Simmons 1986; Tibaldi and Molteni 1990; Tracton 1990; Tibaldi *et al.* 1993, 1994; Colucci and Baumhefner 1998). Additionally, the understanding of processes contributing to the formation or decay of blocking anticyclones is far from complete. In fact, there is no commonly agreed upon (unified) definition of blocking (LS95a). Most published definitions of blocking (e.g. Rex 1950; Shukla and Mo 1983; Lejenas and Okland 1983; LS95a; and others), however, do contain many common elements.

Previous theories on block formation and maintenance have focused on the link to orography and long-wave baroclinic processes (in particular, surface heating) (e.g. Charney and DeVore 1979; Sperenza 1986; Kung *et al.* 1993), interactions between long waves (e.g. Blackmon *et al.* 1977; Austin 1980; Colucci *et al.* 1981; Trenberth and Mo 1985), or the resonant amplification of long waves (e.g. Tung and Lindzen 1979a, b). Early model

\* Corresponding author: Department of Soil and Atmospheric Sciences, 109 Gentry Hall, University of Missouri–Columbia, Columbia, Missouri 65211, USA. email: snrlupo@showme.missouri.edu

studies involved the use of simple, highly truncated, spectral models and were usually discussed within the context of planetary-scale atmospheric flows. Tung and Lindzen described blocking as the resonant amplification of large-scale planetary waves forced by topography and surface heating. They did not address the problems of why blocks occur in preferred geographical locations or why high/low dipoles are the preferred configuration. McWilliams (1980) proposed that blocking could be described as a solitary wave ('soliton', or 'modon'), which in its simplest form resembles dipoles. He showed that the barotropic vorticity equation has solutions that have properties in common with such solitary-wave solutions as, for example, the Kortweg-de Vries equation for waves in a channel. He also showed that blocks have many characteristics in common with 'modons', but he noted that the mean zonal-wind profiles in observed cases might not match those required for 'modons'. He also raised questions about whether a stationary theoretical solution adequately represents the essential dynamics of blocks, which are observed to fluctuate in intensity.

While these studies, and others, describe the presence of blocking in the atmosphere, many other important questions have been raised. For example, blocks, which are planetary-scale phenomenon in both time and space, have been observed to form and decay on time-scales consistent with synoptic-scale events (e.g. Shutts 1983; LS95a, b). The pioneering studies of Kalnay-Rivas and Merkin (1981), Shutts (1983), and Frederiksen (1982, 1983) using various models emphasized the role of mid-latitude transients in the formation and/or maintenance of blocking anticyclones. Included in Shutts's work was an experiment that indicated that these synoptic-scale transients alone were sufficient to produce and maintain a block in an initially zonal flow. Since then, observational studies (e.g. Hoskins *et al.* 1983; Illari 1984; Dole 1986; Mullen 1987; Konrad and Colucci 1988; Tsou and Smith 1990; Alberta *et al.* 1991; Mak 1991; LS95a, b), using a variety of methodologies, have shown the importance of vorticity transport by travelling synoptic-scale disturbances in maintaining the block against the tendency for the block to be advected away by the mean flow. Some of these studies (e.g. Tsou and Smith 1990; Alberta *et al.* 1991; Lupo 1997; Lupo and Smith 1998) also found that temperature advection could also play a role in block formation. Additionally, a few of these studies (e.g. Konrad and Colucci 1988; Tsou and Smith 1990; LS95b) examined the dynamic connection between the development of a particular surface cyclone event and block formation.

The primary objective of this study is to examine, using simple diagnostic techniques, the planetary- and synoptic-scale forcing contributing to the development of a continental blocking anticyclone that occurs over a region and in a season where blocking activity is uncommon, as will be demonstrated using the result of LS95a and others. In particular, this study attempts to determine the extent to which this blocking event is similar to its more commonly (spatially and temporally) occurring counterparts examined in the other studies referenced above on both the planetary and synoptic scales, or whether this event is indeed unique. Also, this paper will utilize two different diagnostic techniques, and demonstrate that the use of both techniques results in similar conclusions and provides a complementary analysis. These techniques will demonstrate that, for this event, the synoptic-scale aspects of block formation are similar to those of other events, despite the rare occurrence of the block over North America and the anomalous planetary-scale flow regime that accompanies it. Also, it is shown that the phase relationship between the block and the upstream cyclones is crucially important in determining whether the block will intensify or decay. The organization of the paper is as follows: section 2 will describe the analyses and diagnostic techniques used in this study. The planetary-scale diagnosis and discussion is covered by section 3. Section 4 will cover the synoptic-scale results, and the paper will be summarized in section 5.

## 2. ANALYSES AND DIAGNOSTIC TECHNIQUES

## (a) Analyses

Two datasets were used for the analyses carried out in this investigation. First, the National Meteorological Center (NMC) (now the National Centers for Environmental Prediction, or NCEP) gridded analyses of geopotential height, temperature,  $u$  and  $v$  (horizontal) wind-vector components, relative humidity, vertical motion (all at selected mandatory levels), and sea-level pressure archived on CD-ROM\* (Mass *et al.* 1987) were used to investigate the role of the planetary-scale forcing in the antecedent conditions leading to this block. The upper-air fields are arranged on grids at selected mandatory levels, while the 500 hPa vertical motions are model six-hour first-guess fields calculated using the NCEP global spectral model. These grids were stored in  $47 \times 51$  point arrays on the NMC octagonal grid, a polar stereographic grid with a resolution of 381 km at  $60^\circ\text{N}$ , and were transformed to a  $2.5^\circ \times 2.5^\circ$  latitude/longitude grid. This dataset was chosen because the software for data manipulation and visualization was already in place, thus facilitating the search for a suitable case-study. Second, the NCEP/National Center for Atmospheric Research (NCAR) re-analyses, available from the NCAR mass-store facilities, were also used, primarily for the synoptic-scale investigation. The NCEP re-analyses (Kalnay *et al.* 1996) used here are  $2.5^\circ \times 2.5^\circ$  latitude/longitude gridded analyses available on 17 mandatory levels (from 1000 to 10 hPa) at six-hour intervals. These analyses† include standard atmospheric variables such as geopotential height, temperature, relative humidity, model-calculated vertical motions ( $\omega$ ),  $u$  and  $v$  wind components, a diverse set of surface fields, and tropopause information. Mandatory pressure-level data were interpolated quadratically in  $\ln[p]$  to 21 isobaric levels in 50 hPa increments from 1050 to 50 hPa. This dataset was chosen because it provided more detailed analyses for the synoptic-scale diagnoses, especially in the vertical.

## (b) Diagnostic techniques

Two techniques were employed in the synoptic-scale investigation of this block. One of these techniques is the ZO equation (Zwack and Okossi 1986), which has been used in several published studies as the diagnostic framework. The ZO equation is a geostrophic vorticity-tendency equation derived in its extended form (Lupo *et al.* 1992; LS95b) by coupling the vorticity and thermodynamic equations through the hydrostatic-thickness equation. The result is an equation that allows for the diagnosis of geostrophic vorticity tendency at a near-surface pressure level as forced by vertically integrated dynamic and thermodynamic forcing mechanisms.

Previous studies have used the extended or complete form of the ZO equation. In the diagnosis of this blocking event, however, a quasi-geostrophic form of this equation is used:

$$\left. \frac{\partial \zeta_g}{\partial t} \right|_{p_L} = PD \int_{p_t}^{p_L} (-\mathbf{V}_g \cdot \nabla \zeta_{ga}) dp - \frac{(PD)R}{f_0} \int_{p_t}^{p_L} \left[ \int_p^{p_L} \nabla^2 \{-\mathbf{V}_g \cdot \nabla T + S(p)\omega\} \frac{dp}{p} \right] dp, \quad (1)$$

\* This work was performed initially using the NMC CD-ROM version II. When version III became available, the work was redone using that version. The visualization software and software to read the CD-ROM can be made available for GEMPAK users by contacting the author.

† For more details on the NCEP re-analyses see Kalnay *et al.* (1996) or consult online information available via the NCAR home page at <http://www.ucar.edu/dss/pub/reanalysis/index.html>

where  $\mathbf{V}_g$  represents the geostrophic wind,  $\zeta_{ga}$  the geostrophic absolute vorticity,  $S(p)$  the static stability parameter ( $-T/\theta \partial\theta/\partial p$ ),  $\omega$  the vertical motion ( $dp/dt$ ),  $\nabla$  the horizontal del operator on an isobaric surface, and  $f_0$  (Coriolis parameter) =  $10^{-4} \text{ s}^{-1}$ ;  $R$ ,  $T$ , and  $\theta$  are the gas constant for dry air, absolute temperature, and the potential temperature, respectively. In (1), the static stability parameter,  $S(p)$ , is a function of pressure only. Also,  $PD$  is  $1/(p_L - p_t)$ , where  $p_L$  represents the near-surface level (the first 50 hPa pressure level above the earth's surface at any grid point) and  $p_t$  is the pressure at some sufficiently high pressure level chosen to encompass most of the atmospheric mass (50 hPa in this study). This simplified form of the ZO equation is used here since the three forcing mechanisms on the right-hand side (vorticity and temperature advection, and adiabatic heating/cooling) are consistently the largest forcing mechanisms at the 500 hPa level. The vorticity tendencies were then relaxed to get height tendencies using sequential overrelaxation (Haltiner and Williams 1980). Height tendencies were examined since the geostrophic vorticities (vorticity tendencies) tend to be weaker in the central region of such planetary-scale phenomena and there is often more than one centre of strong geostrophic vorticity (vorticity tendency) located along the periphery of the height centre (e.g. Sinclair 1996).

The ZO equation is similar to the Petterssen–Sutcliffe equation\* (Petterssen 1956, pp. 320–325), which diagnoses surface development as a function of atmospheric forcing processes occurring between the surface and the non-divergent level, coupling these processes via the thermal wind. However, the ZO equation extends these concepts in order to expose more completely the importance of upper-tropospheric forcing on surface development. This equation is also versatile in that it diagnoses at pressure levels other than the surface can be accomplished simply by solving the geostrophic vorticity-tendency equation (see (3) in Lupo *et al.* (1992)) for some specified level (here, 500 hPa), as was done in LS95b.

Another quantity that is very useful in examining mid-latitude phenomena in a simple and concise manner is potential vorticity, or 'PV thinking'. Ertel (1942) derived an elegant form of this quantity from the hydrostatic primitive equations:

$$P = \frac{\boldsymbol{\omega}_a \cdot \nabla_\theta \theta}{\rho}, \quad (2)$$

where  $P$  is Ertel's potential vorticity (EPV),  $\boldsymbol{\omega}_a$  is the three-dimensional absolute vorticity vector,  $\rho$  is the density of air, and  $\nabla_\theta$  is the three-dimensional del operator on theta surfaces. This form of the potential vorticity has some particularly powerful characteristics in that the potential vorticity is conserved on surfaces of potential temperature in hydrostatic, inviscid, and adiabatic three-dimensional flows (see Pedlosky (1987)). Under these conditions, an examination of the right-hand side of (2) reveals that the dynamic and thermodynamic properties of the atmosphere are contained in one variable,  $P$ . The conservation property is also the foundation for examining wave development in terms of  $\theta$ , or some other conserved variable, on a dynamically significant PV surface (e.g.  $1.5 \times 10^{-6} \text{ K m}^2 \text{ kg}^{-1} \text{ s}^{-1}$ , which is commonly taken to correspond to the dynamic tropopause) (e.g. Hoskins and Berrisford 1988; McIntyre 1988; Nielsen-Gammon and Lefevre 1996). This allows one to examine the important features of atmospheric phenomena in a concise manner. Additionally, as described by Hoskins *et al.* (1985), the global distribution of PV, given a suitable boundary condition and 'reference' state, can be used to determine, or recover, all the relevant dynamical fields such as winds, temperature, and pressure. This powerful property is referred to by Hoskins *et al.* (1985) as the 'invertability principle' for potential vorticity.

\* Equations such as the ZO, omega, and the height tendency equation and the physical interpretation of the forcing processes are referred to in the literature as 'Sutcliffe thinking' as opposed to potential-vorticity diagnostics, or 'PV thinking'.

However, we will examine PV distributions on a pressure surface as described in section 4. We will also study the advection of PV assuming that the quantity  $P$  is a conserved quantity.

### 3. PLANETARY-SCALE ANALYSIS

#### (a) Diagnostics

The blocking anticyclone chosen for this study occurred over North America in late April and early May of 1980, which was during the spring season that preceded the devastating North American drought of 1980 (Dickson 1980; Livezey 1980; Wagner 1980). This blocking event met the criterion for a blocking anticyclone as defined by LS95a, which can be summarized as combining the aspects and advantages of the subjective Rex (1950) definition and the objective Lejenas and Okland (1983) criteria. Comparing the characteristics of this event (Table 1), such as the occurrence, intensity, half-wavelength and duration, to the LS95a sample shows that this block was similar to typical blocking events which occur over land surfaces or in the spring season. However, while this case did have characteristics that were similar to other blocking events, this blocking event can be considered *anomalous* since the event occurred over the North American continent. Figure 1, taken from LS95a (their Fig. 6), and Table 1 show that there were *no* blocking events that occurred over North America from July 1985 through June 1988, meeting the criteria of their climatology. Thus, continental region statistics in Table 1 are due entirely to blocking events that occurred over the Asian continent (see LS95a). Much longer climatologies (see Triedl *et al.* (1981); Lejenas and Okland (1983)) also demonstrate that blocking events are comparatively rare over that portion of the Northern Hemisphere. Additionally, there is also a relative minimum in the occurrence of blocking events during April and May, especially over the eastern Pacific region, as the focus of Pacific region blocking shifts west of the date line (see Triedl *et al.* 1981; LS95a).

An examination of the northern hemisphere teleconnectivity patterns over a seven-week period, beginning about one month before the onset of the block and terminating after the block no longer met the criteria of LS95a (21 March–5 May 1980), was performed using the methodology of Blackmon *et al.* (1984). This one-point correlation analysis provided us with an initial overview of the planetary-scale environment associated with the blocking event. While the time period chosen for the analysis is very short compared to other studies of this type (e.g. Wallace and Gutzler 1981; Mo and Livezey 1986), we feel it is long enough to capture the *essence* of the teleconnectivity pattern that prevailed during the spring of 1980. Our teleconnectivity analysis shown in Fig. 2 corresponds to Fig. 4(f) in Blackmon *et al.* (1984). Since our sample size is smaller, correlations significant at the

TABLE 1. SOME CHARACTERISTICS OF THIS BLOCKING EVENT VERSUS THE MEAN CHARACTERISTICS OF SPRING AND CONTINENTAL (CON) BLOCKING EVENTS IN LUPO AND SMITH 1995a.

Characteristics	Mean Spring Events	Mean CON Events	24 April–4 May 1980
Number of occurrences and as a (%) of total	16 (25.3%)	15 (23.8%)	– (–)
North American occurrences	0 (0%)	0 (0%)	– (–)
Block intensity	3.3	3.5	3.6
Duration	8.2 days	8.7 days	10 days
Half-wavelength	3129 km	3218 km	3463 km

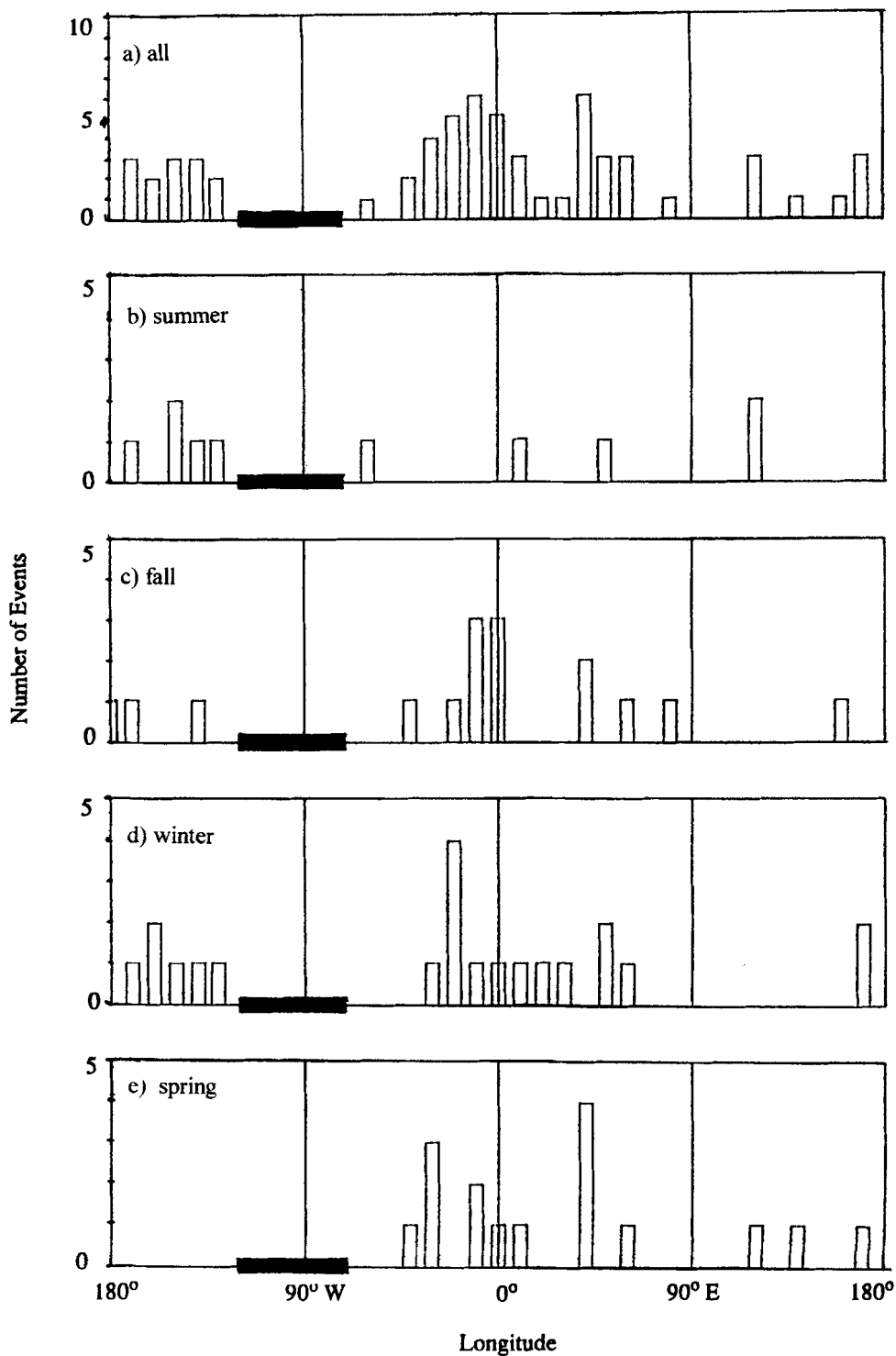


Figure 1. Number of block onset events in ten-degree longitude basins for (a) all, (b) summer, (c) fall, (d) winter, and (e) spring events (taken from Lupo and Smith 1995a). The solid bar represents North America. Note scale difference between (a) and (b)–(e).

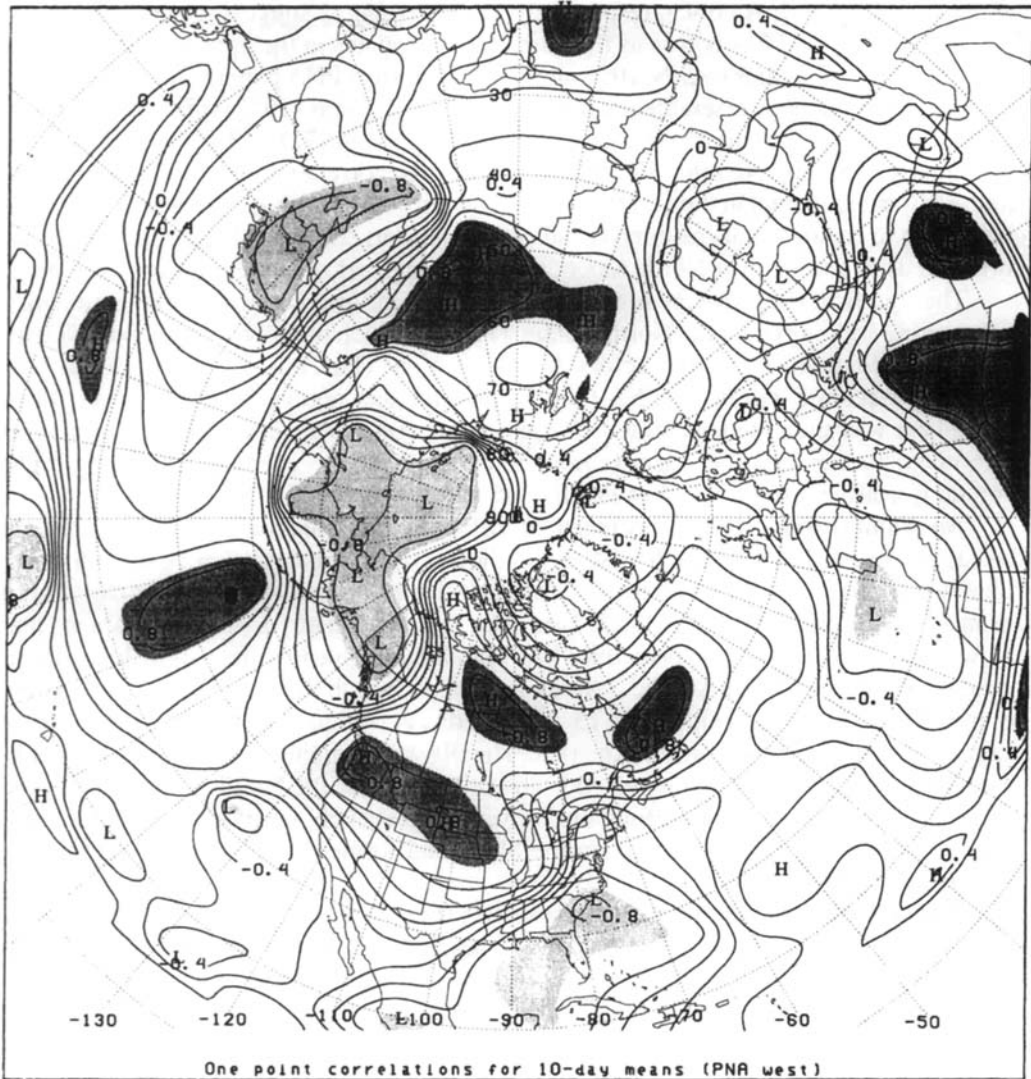


Figure 2. One point correlations using 500 hPa geopotential heights (m) for the period of 21 March to 4 May 1980 over the northern hemisphere. The base point (solid dot) is ( $45^{\circ}\text{N}$ ,  $165^{\circ}\text{W}$ ), and the dark (light) shaded regions are correlations significant at 95%, above 0.75 (below  $-0.75$ ).

95% level, or above 0.75 (below  $-0.75$ ), are darkly (lightly) shaded. The base point for the one-point correlation analysis was chosen to be ( $45^{\circ}\text{N}$   $165^{\circ}\text{W}$ ), which is just upstream of the block chosen for study and its environment. This point also corresponds to the same point used by Wallace and Gutzler (1981) and Blackmon *et al.* (1984) to deduce the Pacific-North American (PNA) teleconnectivity pattern discussed below.

Figure 2 reveals that the teleconnectivity pattern prevalent across the PNA region does *not* correspond to the typical PNA region teleconnectivity found by many other studies. A more *typical* pattern, using the base point mentioned above, (see Blackmon *et al.* (1984) Fig. 4(f) for an example) features a positive correlation between 500 hPa height anomalies over the Gulf of Alaska and south-east North America and a negative correlation to height anomalies over western North America. The most common configuration, for example, is the existence of a 500 hPa trough in the east Pacific and a ridge/trough couplet over

western/eastern North America, respectively. However, Fig. 2 suggests a shorter 500 hPa wavelength over the PNA region as the base point correlates in the opposite manner with 500 hPa height anomalies over North America to the typical PNA pattern described above. However, our data does resemble the pattern shown in Namias (1982) (his Fig. 13(a)) for 700 hPa heights in the summer season (all summers 1947–1972) within the PNA region. The pattern shown by Namias (1982) shows a positive correlation between a base point, similarly located to ours in the east Pacific, and heights over North America and a negative correlation to regions near the continental coastal regions. Namias (1982) stated that this corresponds to a ridge over North America, and a trough off or along each coastal region.

The significant negative (positive) correlations in Fig. 2 suggest lower (higher) heights, or troughing (ridging) over the North (central) Pacific, which broadly defines anomalously strong higher-latitude westerlies across the PNA region. Thus, it is suggested that the prevailing flow regime within the PNA (and North America) region during the seven-week period here was anomalous at least in the sense that: (i) such a pattern would, in a typical year, occur further into the warm season, and (ii) there were anomalously strong high-latitude westerlies over the eastern Pacific and northern Canada.

An examination of the ten-day mean 500 hPa heights and anomalies (Fig. 3(a)) reveals that, at the end of March, a trough existed over the Rocky Mountain region. Also, a blocking ridge was in place over the western and central Atlantic (Fig. 3(a), centred on 26 March) for much of the second half of March. However, Fig. 3(b) (centred on 4 April) shows that the west Atlantic block disappeared by late March/early April while a split flow pattern had developed over North America, which persisted through the first part of April. Then, by mid-April (Fig. 3(c), centred on 15 April) a distinct ridge (western)/trough (eastern) couplet was in place over North America. The 500 hPa heights in Fig. 3(c) also imply that a strong zonally oriented jet extends all the way across the Pacific by this time. The ridge/trough pattern then amplified and moved progressively eastwards until late April (Fig. 3(d), centred on 25 April) when the block had formed (0000 GMT 24 April) over western North America.

The standardized 500 hPa height anomalies (Fig. 3) were constructed relative to the 1960–1994 500 hPa monthly-mean heights using the data obtained from the NCEP CD-ROM. These long-term mean-height fields were interpolated linearly in time to match each corresponding ten-day period in Fig. 3, and then subtracted from the ten-day mean-height field. The height anomalies were then divided by the standard deviation of the 500 hPa height field. The standard deviations were constructed using monthly-mean height data found on the CD-ROM and thus provide a rough estimate of this quantity. However, it should be cautioned that these standard deviations of the corresponding 500 hPa height fields are smaller than those constructed using daily height fields. Also, the discussion is limited, in most cases, to anomalies of greater (less) than 2.0 (–2.0) standard deviations.

In the latter half of March, there was a large positive height anomaly (Fig. 3(a)) associated with the block over the western Atlantic. There was also a weaker positive height anomaly located over the eastern Pacific (not shaded). Additionally, a region of low heights also persisted over south-western North America. Within the next period (Fig. 3(b)), all of these anomalies weakened over the North American region as part of the western Atlantic positive anomaly tracked westwards (following the labelled centres) into western North America. It is also likely that the east Pacific region height anomaly also moved north-eastwards into western North America as well, becoming superposed with the Atlantic anomaly. Examining the intervening ten-day running-mean maps, which are not shown for brevity, supported our interpretation. This positive height-anomaly centre then amplified over western and central North America throughout the rest of April (Figs. 3(c) and (d)) and into May, which included the block lifetime. There was also a large negative

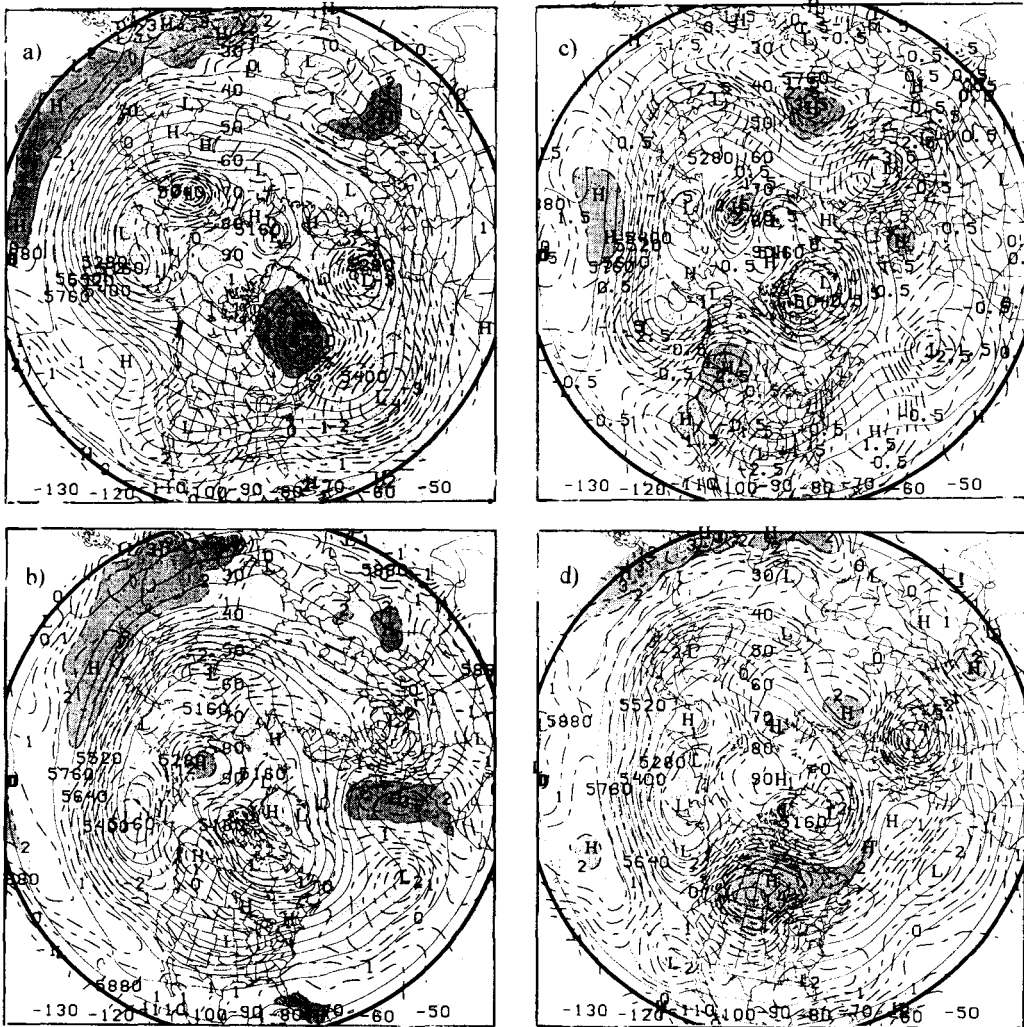


Figure 3. Ten-day running mean of northern hemisphere 500 hPa heights (m, solid) and standardized height anomalies (dashed) with a five-day overlap for (a) 21–30 March, (b) 31 March–9 April, (c) 10–19 April, and (d) 20–29 April 1980. The contour intervals are 60 m and 0.5 standard deviations in the height and anomaly fields, respectively. Dark (light) shading indicates height anomalies greater than 2.0 (–2.0) standard deviations.

height anomaly present over the eastern and central Pacific throughout the seven-week period (Figs. 3(a)–(d)). Thus, Fig. 3 suggests the existence of an anomalously strong and more eastwardly extended jet with respect to normal throughout this period with the presence of a positive anomaly in the equatorial regions south of a negative anomaly over the North Pacific (as suggested by Fig. 2). The negative height anomaly will be discussed in more detail later in this section. Finally, examining the 30-year-mean height fields for April (Fig. 4(a)) reveals a tendency for weak split flow over western North America during April. Also, the previous analysis of the 500 hPa height fields and height anomalies for March and April 1980 suggest that the occurrence of such an amplified large-scale ridge over North America at this time is anomalous.

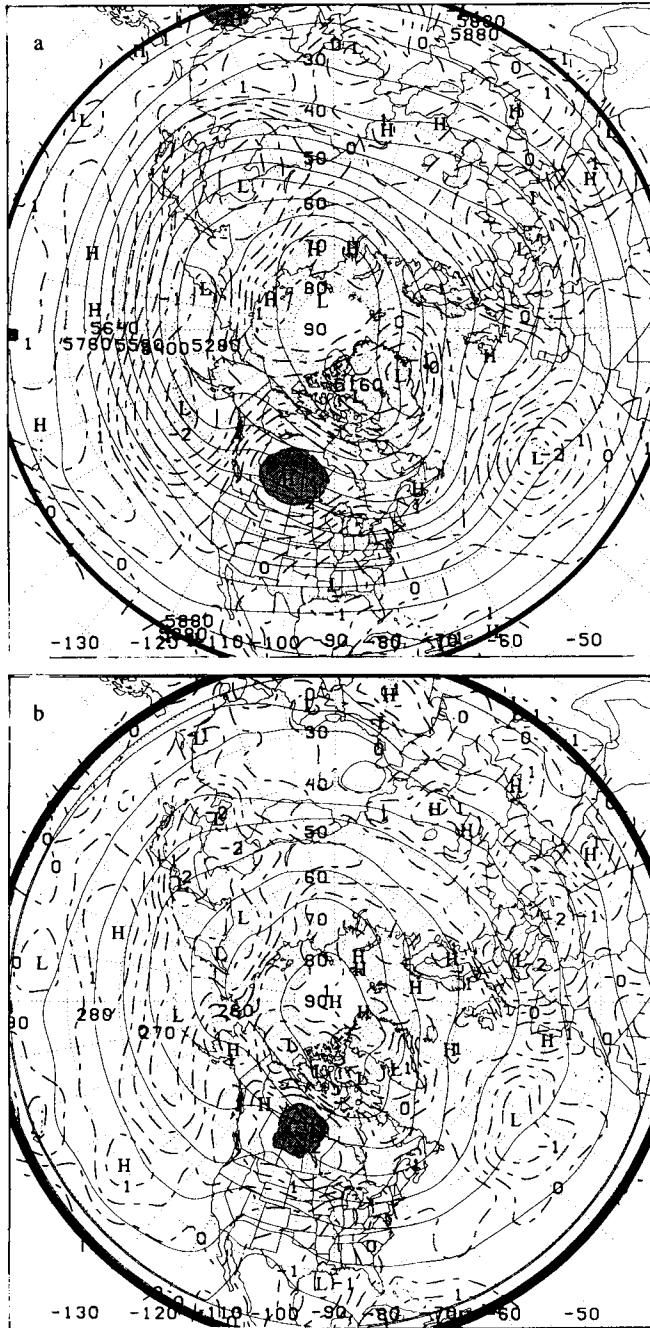


Figure 4. Mean (a) 500 hPa heights (m, solid) and (b) 850 hPa temperatures (K, solid), and standardized anomalies (dashed) for the month of April (a) 1960–1994, and (b) 1964–1994. Dark (light) shading indicates height anomalies greater than 2.0 ( $-2.0$ ) standard deviations.

*(b) Discussion*

Further analysis was carried out in order to support the above contention that this blocking event was associated with a flow regime in which the climatological planetary-scale 500 hPa features were more amplified and/or phase-shifted relative to the climatological means. Figure 4(a) strongly suggests that wave numbers 2 and 3 dominate the climatological April 500 hPa height field over North America. The 500 hPa heights and standardized height anomalies associated with the anomalous ridging over North America throughout April (Figs. 3(b)–(d)) also suggest dominant wave number 2 to 4 patterns. The April 1980 500 hPa height anomalies (Fig. 4(a)) corroborate the presence of a wave number 2 and 3 pattern during that month. Also, the standardized anomaly maxima and minima imply that the regular northern hemispheric trough/ridge features are amplified and/or shifted downstream of their climatological position especially over North America, the Atlantic, and into western Europe. The presence of amplified wave numbers 1, 2, and 3 in association with blocking have been noted by many investigators (e.g. Austin 1980; Colucci *et al.* 1981; Trenberth and Mo 1985), suggesting a prominent role for planetary-scale forcing in the development and maintenance of blocking anticyclones. Other studies have noted the presence of travelling wave numbers 1 and 2 in association with blocking (e.g. Quiroz 1987; Lejenas and Madden 1992). Figure 3 may lend support to these observations since the height anomalies associated with the Atlantic block earlier in the period are seen to ‘migrate’ westwards with time into the North America region. However, the 500 hPa height field and height anomalies would have to be decomposed into their component wave numbers in order to confirm this observation.

Several processes may have contributed to the anomalous ridging in the 500 hPa heights over North America described above. The study of the North American drought of 1980 by Namias (1982) provides some insight. He examined some of the antecedent general-circulation features that presaged the occurrence of this summer drought and other North American summer droughts in more detail (Namias 1982, 1983). Specifically, he found that sea surface temperatures (SSTs) were much lower than normal over most of the central North Pacific for a period of several months leading up to the summer of 1980, and his Fig. 10(a) shows the extent of these low SSTs for May 1980. This cold pool may be manifested by the persistence of large negative 500 hPa height anomalies in March and April (see Fig. 3). The extent to which the cool SSTs are entirely responsible for the 500 hPa height anomalies cannot be assessed briefly here. However, modelling studies (e.g. Kung *et al.* 1993; Nakamura *et al.* 1997) have demonstrated that Pacific region SSTs can produce 500 hPa height anomalies similar in magnitude to those shown here. These negative anomalies typically correspond to a stronger and an eastwardly extended Pacific jet (e.g. Hurrell 1996). Figure 5 is an example of the conditions that prevailed in the 250 hPa wind field during this study period (as suggested by Figs. 2 and 3). The shaded regions in Fig. 5(a) depict where the ten-day mean 250 hPa wind speeds are greater than  $35 \text{ m s}^{-1}$ . Note that the strong jet extended all the way across the Pacific Ocean and into North America. The map of standardized wind anomalies (Fig. 5(b)) demonstrates that the stronger than normal westerlies (dark shading) across the entire Pacific and into North America during this season were anomalous. The planetary-scale (in time and space) negative 500 hPa height anomaly found in Fig. 3 may be similar to zonally elongated planetary-scale eddies found by Hoskins *et al.* (1983) over the Pacific region of the northern hemisphere during the preceding winter (1979–80). They showed that these planetary-scale eddies contributed to the strengthened Pacific jet in the exit region (‘smeared’ the jet out). These planetary-scale eddies have a quasi-barotropic structure and are capable of displacing the prevailing westerlies and could increase the kinetic energy of higher-frequency transients (Hoskins

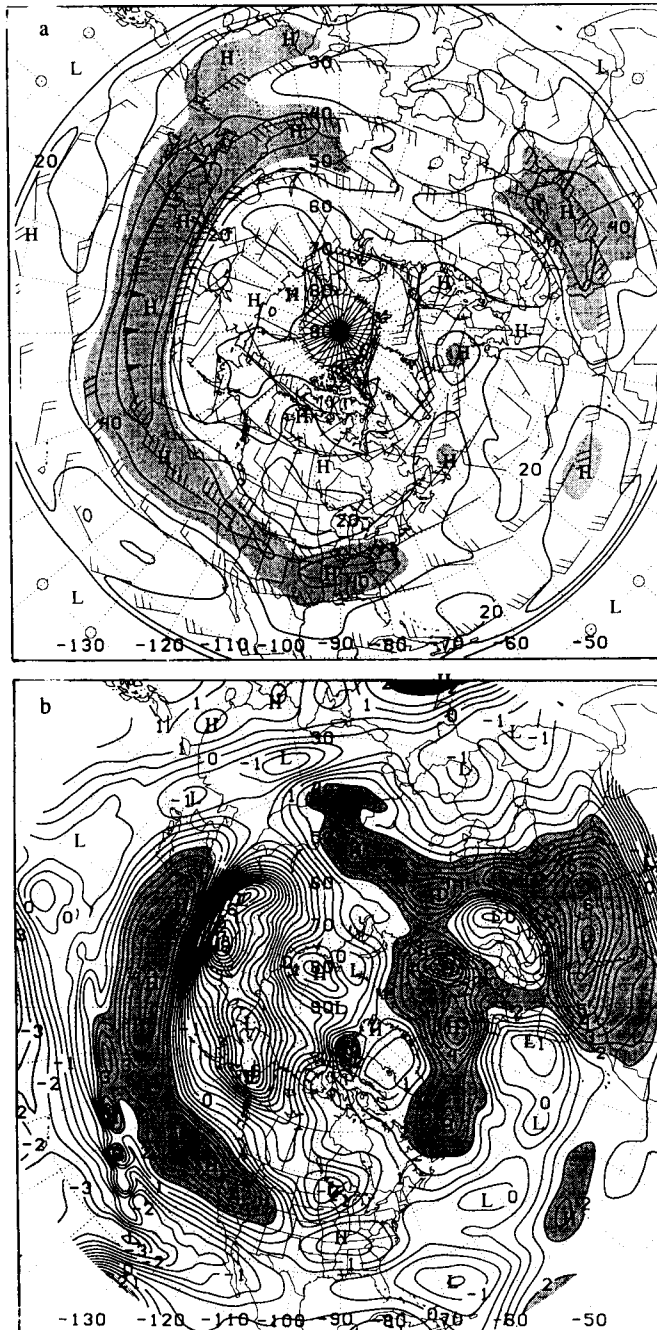


Figure 5. The (a) mean 250 hPa wind speeds ( $\text{m s}^{-1}$ ) for 5–14 April 1980, and (b) standardized wind-speed anomalies. The contour interval is (a) 10 ( $\text{m s}^{-1}$ ), and (b) 0.5 standard deviations. The shading convention is (a) wind speeds greater than 35 ( $\text{m s}^{-1}$ ), and (b) dark (light) shading height anomalies greater than 2.0 (–2.0) standard deviation. On the wind barbs in (a), a full feather (flag) represents 10 (50) ( $\text{m s}^{-1}$ ).

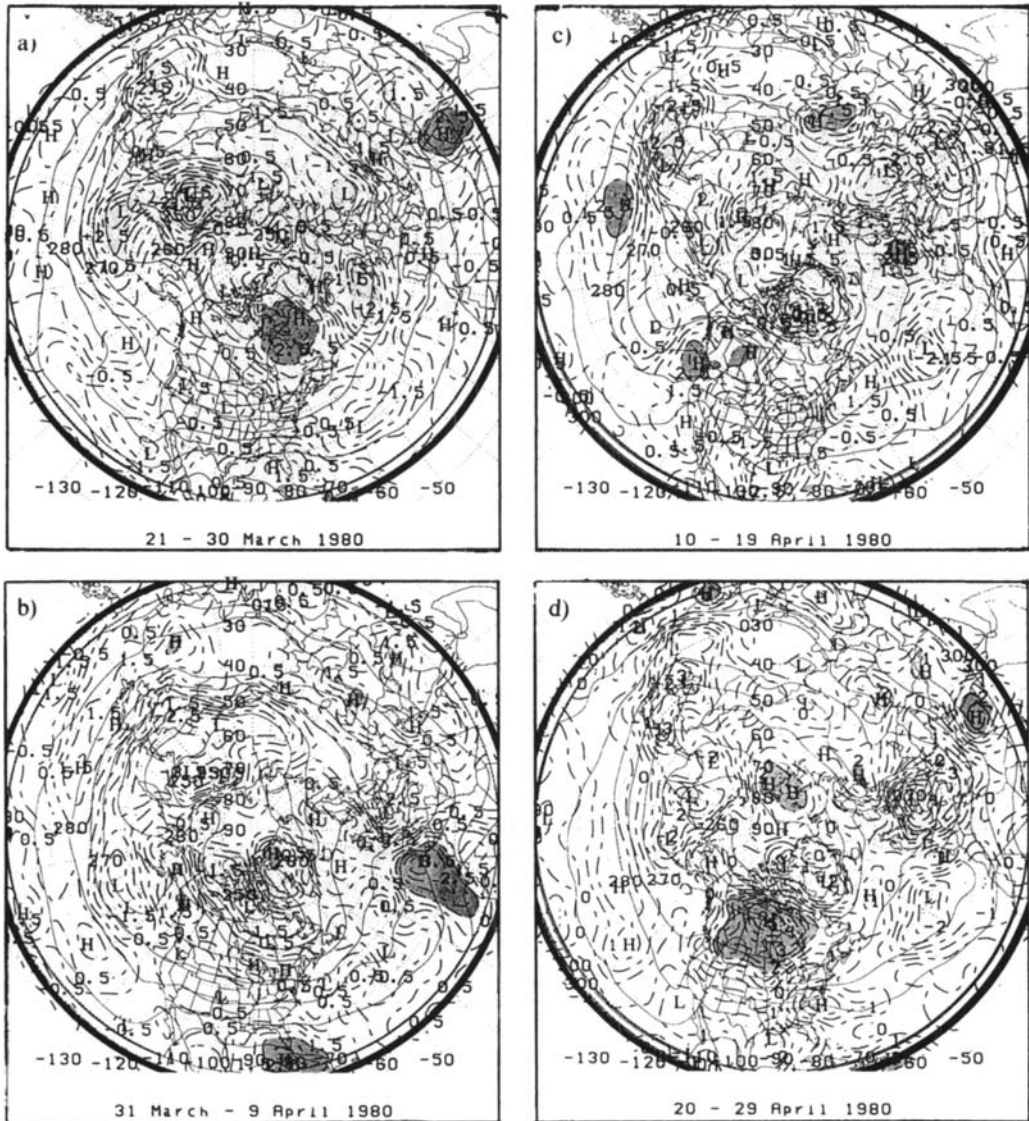


Figure 6. Same as Fig. 3 except for 850 hPa temperatures (K). The contour intervals are 5 K and 0.5 standard deviations for the temperature and anomaly fields, respectively.

*et al.* 1983), which in turn can impact on the evolution of the planetary-scale features (Simmons *et al.* 1983). Finally, the eastwardly extended Pacific jet found here would then result in the diffluent jet exit region, and consequently the upstream ridging, being displaced further eastwards than normal as is generally shown by Figs. 3 and 5.

The above discussion may partially explain the presence of anomalous ridging over North America. Further analysis, however, was conducted using the 850 hPa temperatures and standardized anomalies (Fig. 6) in order to gain more insight into the process responsible for the 500 hPa ridging. Figure 6 was constructed in the same manner as the 500 hPa heights and anomalies shown in Figs. 3 and 4. The 850 hPa level was chosen since

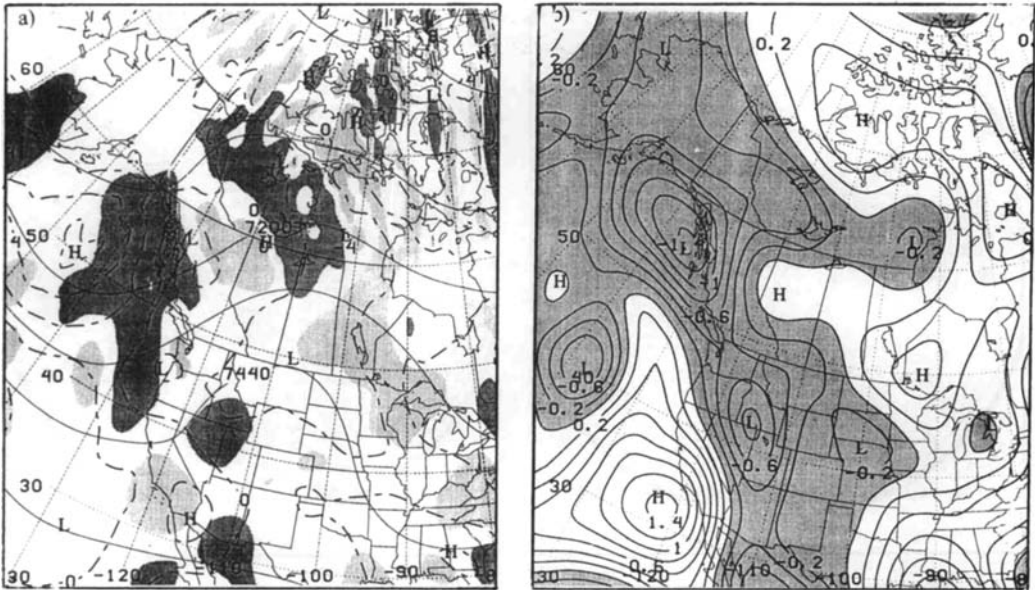


Figure 7. Mean (a) 700–200 hPa thicknesses (m, solid), and 500 hPa geostrophic vorticity ( $1.0 \times 10^{-5} s^{-1}$ , dashed), and (b) vertical motion in  $\mu b s^{-1}$ . Contour intervals are 60 and 2 in (a), and 0.2 units in (b), respectively. Dark (light) shaded regions in (a) are vorticity advection by the thermal wind greater (less) than  $\pm 3.0 \times 10^{-9} s^{-1}$ , and the shading in (b) represents upward motion.

lower-tropospheric heating would cause ridging at 500 hPa in the absence of upper-level cooling. At 850 hPa, temperatures were higher than average over much of northern Canada (and eventually all of North America) for the entire analysis period, especially after mid-April. However, it was not until mid-April that temperatures were significantly higher over the middle portion of North America (Fig. 6(c)) and along the Pacific north-west as the 500 hPa ridge became well established over western North America (Fig. 3(c)). These observations are supported by Fig. 4(b), which shows the 850 hPa temperature anomalies for the month of April 1980 and 30-year mean 850 hPa temperatures for April. Typically, a thermal ridge/trough couplet exists over the western/eastern portion of North America, respectively. The first half (Figs. 6(a) and (b)) of our analysis period reflects a similar distribution, while in the latter half of the period there was a distinct thermal ridge over North America (Figs. 6(c) and (d)). The surface temperatures (not shown) for April 1980 also show a large positive anomaly (greater than 4 degC over central Canada) over North America. Finally, a comparison of the 850 hPa temperatures (Figs. 6(c) and (d)) and heights (not shown) to the 500 hPa heights (Figs. 3(c) and (d)) over the same period suggests that the anomaly associated with mean ridge over North America had a strong equivalent barotropic component.

A simple Sutcliffe-type diagnosis was performed in order to gain further insight into the formation of this 850 hPa temperature anomaly over North America. A representative ten-day average is shown in Fig. 7. This period was chosen since it is the first full ten-day period that follows the amplification of the 500 hPa ridge and encompasses block onset. Figure 7(a) shows the 700–200 hPa thicknesses plotted over the 500 hPa geostrophic relative vorticity. The 500 hPa vertical motion is shown in Fig. 7(b). The advection of vorticity by the thermal wind (shaded regions in Fig. 7) is similar in form to the ‘development’ term in the Sutcliffe equation, or the ‘Sutcliffe development formula’ (e.g. Holton 1979,

TABLE 2. THE THERMODYNAMIC BUDGET FOR THE REGION BOUNDED BY 45°N, 70°N, 130°W AND 80°W OVER THE PERIOD 15–24 APRIL 1980 IN K d<sup>-1</sup>.

Temperature advection	Adiabatic	Latent heat	Sensible heat	IR heating	Total
Term (b)	Term (c)	Term (d) LHR	Term (d)	Term (d) IR	Term (a)
1.19	0.07	0.14	0.03	-0.72	0.71

(a), (b), (c) and (d) refer to terms in Eq. (3).  
IR = infrared, LHR = latent-heat release.

p. 224). Thus, the regions of cyclonic (anticyclonic) vorticity advection by the thermal wind in Fig. 7 represent regions of surface cyclone (anticyclone) development in the time-mean sense. Upstream surface cyclone development prior to block onset is an important ingredient to block formation as found by Tsou and Smith (1990) and others. There is also a correspondence between regions of mean upward (downward) motion (Fig. 7(b)) and mean cyclonic (anticyclonic) vorticity advection by the thermal wind in Fig. 7(a). This suggests that anticyclonic-vorticity advection by the thermal wind and the accompanying subsidence regions over central North America may have played some role in the formation of the anomalous 850 hPa warmth.

To support the above suggestion, further analysis of the anomalous 850 hPa warmth over North America was accomplished using the thermodynamic equation in the form:

$$\left. \frac{\partial T}{\partial t} \right|_{850} = \left( \begin{array}{c} \text{(a)} \\ \text{(b)} \\ \text{(c)} \\ \text{(d)} \end{array} - \mathbf{V} \cdot \nabla T + S\omega + \frac{\dot{Q}}{c_p} \right)_{850}, \quad (3)$$

where terms (b) and (c) represent the mean contributions from temperature advection and adiabatic warming/cooling, respectively, with  $\mathbf{V}$  the 850 hPa wind velocity. Term (d), the mean diabatic heating term, with  $c_p$  the specific heat at constant pressure, contains contributions from latent-heat release, boundary-layer sensible heating/cooling, and infrared heating/cooling processes. The parametrization of each quantity in (d) is described in LS95b. In Table 2, instantaneous calculations of each term (b), (c), and (d) were averaged in time (15–24 April) and space (bounded by 45°N, 70°N, 130°W, and 80°W or northern North America). The time period chosen corresponds to the Sutcliffe analysis presented above, and the region corresponds to the area of anomalous 850 hPa warmth (see Fig. 6(f)). The total heating rate (a) is the sum of each term. Table 2 shows that the mean temperature advection was the primary process responsible for anomalous warmth at 850 hPa. However, this mechanism would tend to produce upward motion at 850 hPa and adiabatic cooling. Thus, anticyclonic-vorticity advection producing subsidence as shown in the analyses above, in conjunction with the mean infrared cooling (producing downward motion), resulted in the adiabatic warming, which must have been sufficient to produce the net warming in term (c). Thus, based on the simple thermodynamic and Sutcliffe analyses above, the anomalous warmth at 850 hPa would seem to be produced primarily by the mean temperature advection and the mean subsidence associated with anticyclonic-vorticity advection by the mean thermal wind.

#### 4. SYNOPTIC-SCALE ANALYSIS

In this section, we use both ‘Sutcliffe’, and ‘potential vorticity’ (PV) thinking in order to show that they can be used in a complementary fashion. The 300 hPa EPV fields were

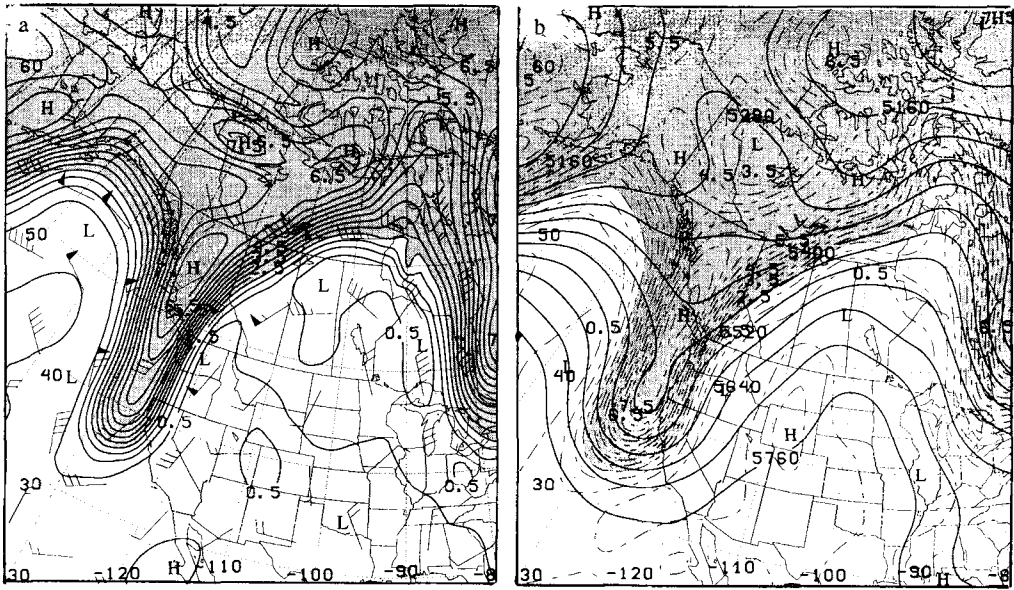


Figure 8. Horizontal distribution of Ertel potential vorticity ( $1.0 \times 10^{-6} \text{ K m}^2 \text{ kg}^{-1} \text{ s}^{-1}$  or potential vorticity units) on the (a) 315 K (solid), and (b) 300 hPa (dashed) surface for 0000 GMT 21 April 1980. The solid contours in (b) are geopotential height (m). The contour intervals are (a) 0.5 PVU and (b) 60 m, and values greater than 2.0 PVU are shaded. Wind barbs in (a) are as in Fig. 5.

calculated using the NCEP re-analyses and will be examined and displayed on the 300 hPa pressure surface (e.g. Bosart and Lackmann 1995). Maps of EPV on the  $\theta = 315 \text{ K}$  surface and the 300 hPa pressure surface for 0000 GMT 21 April 1980 are compared (Fig. 8). The 315 K level was chosen since it is close to the 300 hPa level in the mid-latitudes (see Hoskins *et al.* 1985). The important features look very similar in a qualitative sense. The 300 hPa wind and the 500 hPa height field, superimposed on Figs. 8(a) and (b), respectively, also imply that the advection of PV should be similar. While the conservation property of PV is sacrificed, this comparison shows that EPV calculated on a pressure surface can still be used effectively as a diagnostic tool. Also, Hoskins *et al.* (1985) comment that, since pressure and height are the vertical coordinate for the observation network, it is necessary to use numerical interpolation to calculate PV on isentropic surfaces. Thus, even PV fields calculated on isentropic surfaces are still only approximations to the real PV distribution.

A brief overview of the block life cycle reveals that there were two periods of intensification separated by a (mid-life) decay period (Fig. 9). The initial intensification period was more robust and resulted in the maximum intensity being achieved 72 hours after onset, which was similar to the life cycle of an Atlantic-region blocking event studied in Lupo (1997). In this section, these intensification periods, as well as the development period, will be associated with upstream cyclone development (e.g. LS95b; Lupo 1997). It will also be shown that there may be an optimum phase relationship between the developing cyclone and the block.

#### (a) Block development

Figure 10 displays the 500 hPa heights and 300 hPa winds throughout the block-formation period. All the key elements of the Tsou and Smith (1990) block-formation mechanism were present: (i) a planetary-scale quasi-stationary 500 hPa ridge over North

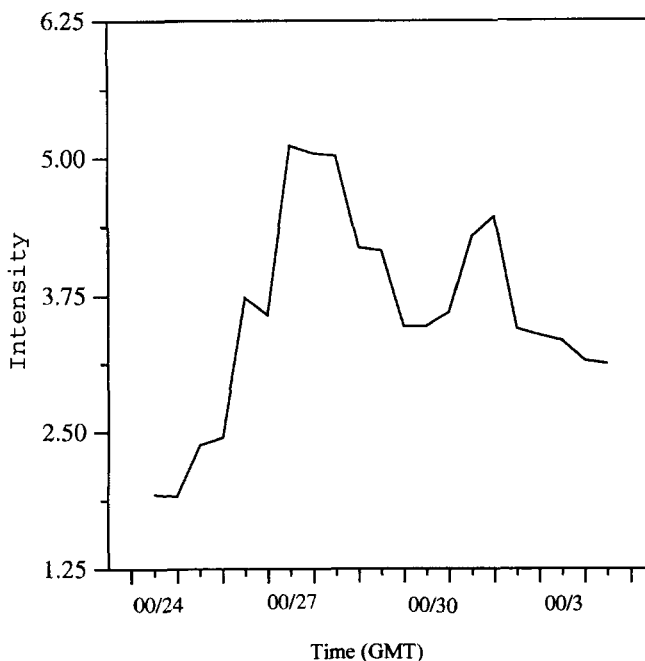


Figure 9. Block intensity (BI) versus time from block onset to termination. BI is calculated by multiplying a normalized height value at the block centre by 100 such that BI is a number between 1 and 10, with 1 being the least intense. Onset and termination are defined by the block satisfying a combination of the Rex (1950) and Lejenas and Okland (1983) criteria simultaneously. See Lupo and Smith (1995a) for more details.

America (Fig. 10), (ii) a developing precursor upstream surface cyclone (Figs. 10(b)–(i)), (iii) an associated 500 hPa amplifying, upstream short-wave ridge (Fig. 10(c)–(h)), and (iv) a strong jet maximum on the upstream flank of the developing short-wave ridge located just off the western coast of North America (Figs. 10(c)–(h)). Tsou and Smith (1990) and LS95b noted the presence of one precursor surface cyclone in association with block formation. However, in this case, there were two identifiable upstream surface cyclones (L1 and L2) that may have contributed to block formation. The cyclones were located approximately  $60^{\circ}$  and  $40^{\circ}$  longitude upstream of the planetary-scale ridge axis when they began a period of rapid development, and this is similar to the findings of LS95a who noted that these cyclones tended to be located about  $10^{\circ}$ – $50^{\circ}$  longitude upstream of the developing block. L1 deepened rapidly after 0000 GMT on 20 April (started at 989 hPa and deepened 22 hPa in 36 hours) and was located just south-west of the Aleutians at that time (Fig. 10(a)). This cyclone moved into south-west Alaska over the next 48 hours. At 500 hPa, the short-wave ridge began to amplify markedly after 1200 GMT 21 April (Fig. 10(d)).

The ZO calculated height tendencies (Fig. 11(a)) reveal that strong height rises were located over the amplifying short-wave ridge. These height rises were mainly due to anticyclonic-vorticity advection (Fig. 11(b)), with minor contributions from the thermal-forcing mechanisms (not shown), a result similar to those of LS95b. The same analysis using PV diagnostics (Fig. 11(c)) shows the poleward extrusion of low-PV air over the eastern Gulf of Alaska and western Canada, and subsequent low-PV advection into the region of the developing ridge over British Columbia, in a similar manner to that described by Illari (1984). The strong negative PV advection is shown quantitatively at 300 hPa (Fig. 12(a)) over western Canada.

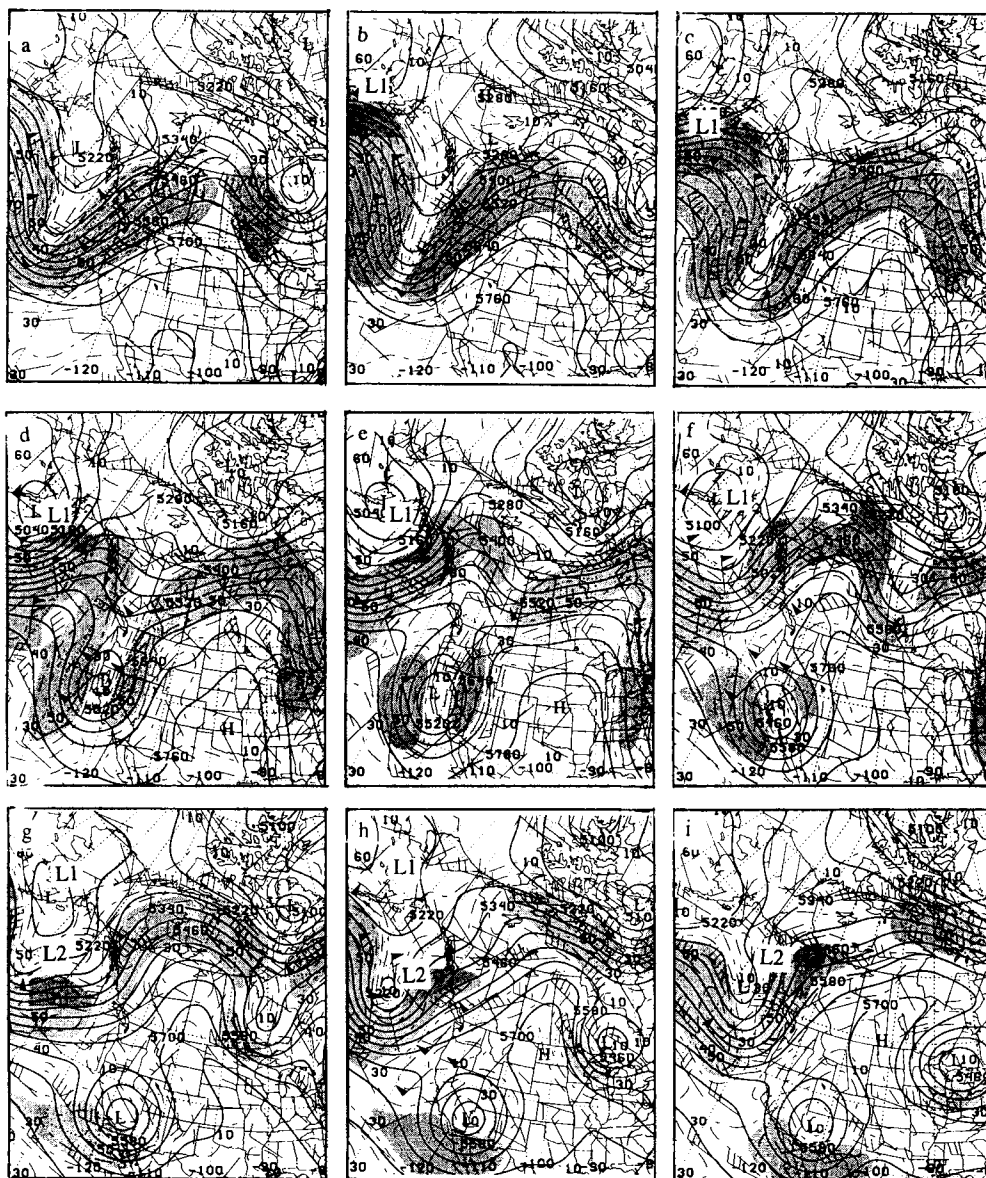


Figure 10. Horizontal distribution of 500 hPa (m) and 300 hPa wind ( $\text{m s}^{-1}$ ) for (a) 0000 GMT 20 April 1980, (b) 1200 GMT 20 April, (c) 0000 GMT 21 April, (d) 1200 GMT 21 April, (e) 0000 GMT 22 April, (f) 1200 GMT 22 April, (g) 0000 GMT 23 April, (h) 1200 GMT 23 April, (i) 0000 GMT 24 April. The heights (solid) are contoured every 60 (m), and the winds (dashed) are contoured every 10 ( $\text{m s}^{-1}$ ) and shaded for values above 35 ( $\text{m s}^{-1}$ ). The wind barbs show wind direction and each feather and flag represents 10 ( $\text{m s}^{-1}$ ) and 50 ( $\text{m s}^{-1}$ ) increments, respectively. Relevant surface lows are marked with an 'L1' or 'L2'; all others are upper air markers.

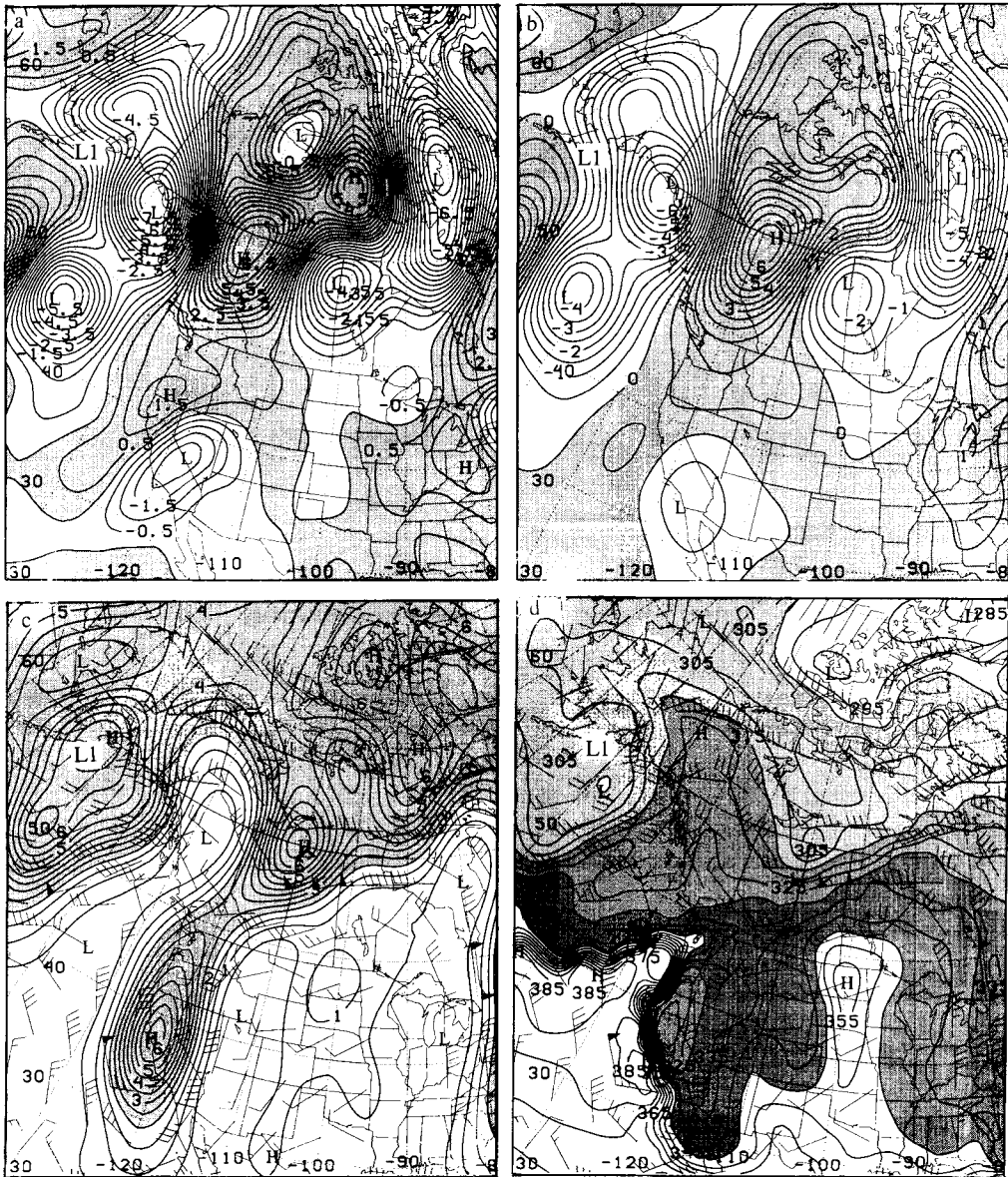


Figure 11. Calculated ZO height tendencies ( $\text{m s}^{-1}$ ) at 500 hPa for 0000 GMT 22 April 1980 of the (a) total, and (b) vorticity advection. The height tendencies are contoured every  $5.0 \times 10^{-4}$  ( $\text{m s}^{-1}$ ) and positive values are shaded. Horizontal distributions of (c) Ertel potential vorticity (PVU), and (d) tropopause potential temperature (K) at 0000 GMT 22 April 1980. Contour intervals are (c) 0.5 PVU and (d) 5 K. Shading conventions are: (c) values greater than 2.0 PVU and (d) light (medium) [dark] values between 300 and 315 (315 and 330) [330 and 345] K. The wind bars are the same as in Fig. 10. Surface lows are marked with an 'L1' or 'L2'.

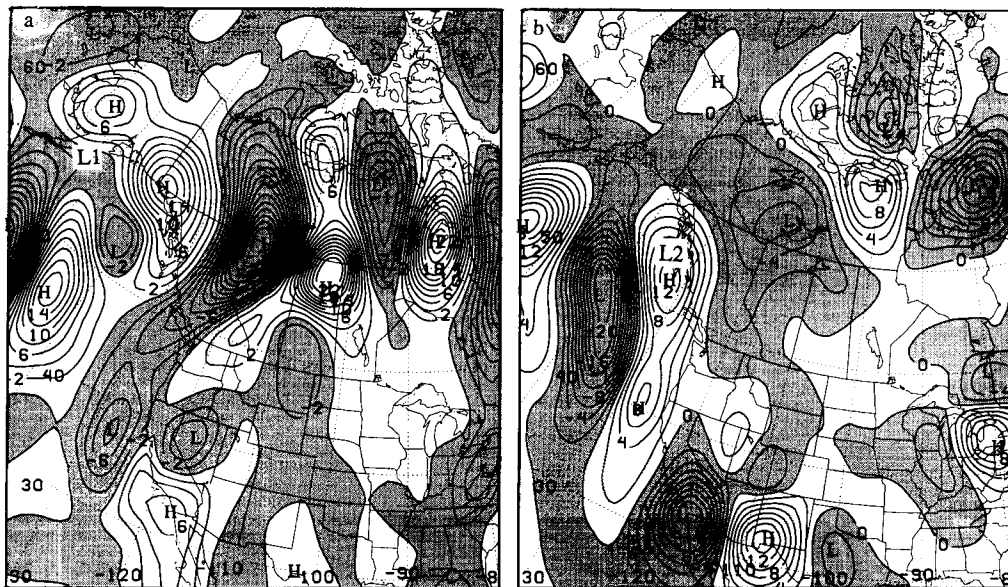


Figure 12. The horizontal distributions of the 300 hPa advection of potential vorticity ( $2 \times 10^{-11}$  PVU  $s^{-1}$ ) for (a) 0000 GMT 22 April and (b) 0000 GMT 24 April 1980. The shaded regions represent negative PV advection.

There are other features in the 300 hPa PV field that are important to identify. For example, the upstream extrusion of high-PV air over the Gulf of Alaska extended equatorwards deep into the mid-latitudes. This region of high-PV air located along the west coast of North America that was about to fracture from the main PV reservoir at this time was slightly tilted south-west to north-east, which resembled anticyclonic wave breaking as described by Thorncroft *et al.* (1993). They found that this type of wave breaking is commonly associated with blocking. Lastly, the precursor quasi-stationary planetary-scale ridge feature shown in Fig. 10 over central North America was evident in both EPV fields (Figs. 11(c) and (d)) (see the corresponding regions of low EPV values associated with the ridge). Also evident are the corresponding warm dynamical tropopause regions associated with both the planetary- and synoptic-scale ridges described above.

The second surface cyclone (L2) began to develop around 0000 GMT 23 April (started at 995 hPa and deepened 7 hPa in 24 hours) and was located in the eastern Pacific off the coast of North America (Fig. 10(g)). This cyclone was a modest developer that moved over the British Columbia coast by 1200 GMT 24 April. After this time, the second surface cyclone was 'absorbed' by a larger, stronger cyclone following immediately behind it over the eastern Pacific. At 500 hPa on 0000 GMT 24 April (Fig. 10(i)), or block onset as defined by LS95a, note the presence of another short-wave ridge on the north-west side of the block over British Columbia. Using the ZO diagnostics, (Fig. 13(a)) shows that, at that time, there were still height rises occurring over the north-west portion of the block, including the short-wave ridge. Height rises were also occurring over much of the incipient block located over North America. Again, these height rises were dominated by anticyclonic-vorticity advection (Fig. 13(b)). However, temperature advection contributed more significantly to the height-rise region over the north-west corner of the block, and consequently the short-wave ridge in Fig. 10(i) (not shown), than in the previous sequence. The PV maps (Fig. 13(c)) imply that there were regions of low PV on the western flank of

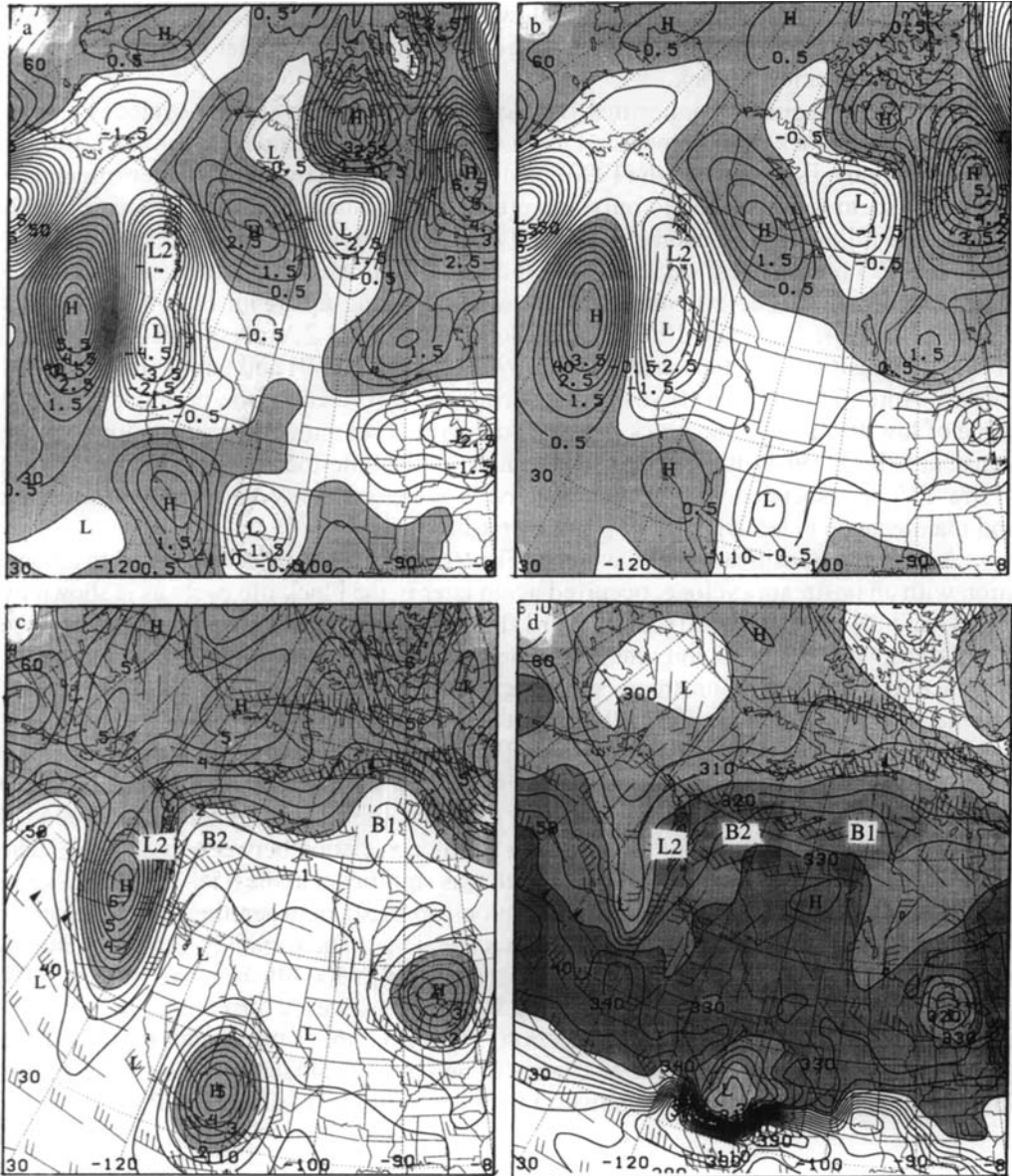


Figure 13. Same as Fig. 11, except for 0000 GMT 24 April 1980. 'B1' and 'B2' are perturbations associated with their respective surface lows.

the block with low values being advected into the blocked region. The upstream high-PV air (Fig. 13(c)) extruded deep into the mid-latitudes and eventually 'fractured' as in Fig. 11(c). In Fig. 13(c), there were two perturbations (B1 and B2, corresponding to L1 and L2, respectively) or regions of low EPV, on the north-west and north-east flanks of the block. An examination of the intervening maps (not shown) reveals that each region corresponded to each of the two upstream precursor cyclones. Figure 13(d) also demonstrates that the tropopause was warmer in the blocked region and the two perturbations noted in the PV

fields are evident. Also, there was a high/low couplet over central North America in the dynamic tropopause  $\theta$  field that corresponded to the high/low couplet in the height field (Fig. 10(i)), indicating a block.

Thus, this diagnosis implies that two developing upstream surface cyclones can be associated with block development in this case. Therefore, the paradigm for block formation put forth by Tsou and Smith (1990), and expanded upon by LS95b (intensification), would not seem to be limited to only one precursor cyclone. In fact, in association with the cyclone following L2, another poleward extrusion of low-PV air (and corresponding calculated ZO height rises) occurred, and the low-PV air was (not shown) advected into the blocked region. These features can be seen occurring upstream of similar features described in Figs. 13(a) and 12(b). The cyclone, following L2, corresponded to a period of block intensification after onset (as in LS95b and see Fig. 9) and culminating at 0000 GMT 27 April. Thus, it can be seen that, during block formation, the periodic poleward surge of low-PV air into the block is associated with developing upstream synoptic-scale transients. Illari (1984) discussed the continuous (in the time-mean sense) poleward surge of low-PV air associated with upstream synoptic-scale transients during block formation and maintenance in her analysis of a summer-season case.

A brief re-intensification of the block (Fig. 9), after 0000 GMT 30 April and in association with an upstream cyclone, occurred again later in the block life cycle as is shown by the ZO and PV maps for 0000 GMT 30 April (Fig. 14). Many of the same features that were found during development and intensification could also be seen in Fig. 14, including the presence of a developing upstream surface cyclone, calculated 500 hPa ZO height rises, and the 300 hPa advection of low-PV air on the upstream flank of the block. Additionally, the calculated ZO height rises and negative PV advection (Figs. 14(a) and (d)) were collocated over the eastern Pacific and western North America. Correlating the calculated ZO height tendencies and the PV advection over the block lifetime and in the region bounded by 30°N, 70°N, 150°W and 90°W, reveals a strong correlation between these fields. The correlation coefficient averaged  $-0.67$ , which was significant at the 95% level. A Z-score test assuming the null hypothesis, or no relationship exists between the two (Neter *et al.* 1988), was used here and elsewhere as the statistical test. The negative correlation means that calculated 500 hPa ZO height rises (falls) correlate to 300 hPa negative (positive) PV advection. Both 500 hPa ZO height rises and 300 hPa negative PV advection can be associated with block formation and intensification. This also implies that, under the conditions of PV conservation, the local rate of change in heights, as calculated by the ZO equation in this study, should correlate (negatively) with the local rate of change in PV.

#### (b) *Maturity*

The maximum intensity attained by this blocking event occurs around 0000 GMT 27 April (Fig. 9). After this time, the block lost some of its intensity. The ZO height-tendency calculation (Fig. 15(a)) shows that the forcing at the block centre was weak and the strong height-tendency regions were located away from the block centre. Also, in contrast to the development and intensification stage, there were no significant surface cyclones located upstream of the block (Fig. 15(c)) (within 60° longitude). This observation concurs with the maintenance period of the LS95b case. The EPV distribution also corroborates the lack of strong forcing at the block centre. Also, there are no broad areas of low PV located in the block at this time (Fig. 15(b)), and regions of strong low-PV advection were located too far upstream to impact on further block intensification (Fig. 15(d)). In fact, a region of higher EPV ( $1.5+$  PVU) and positive PV advection were located near the block centre, or over the front-range region, at this time. Tracing the evolution of the high-PV perturbation indicates that the PV fragment that had fractured off the main reservoir was located over

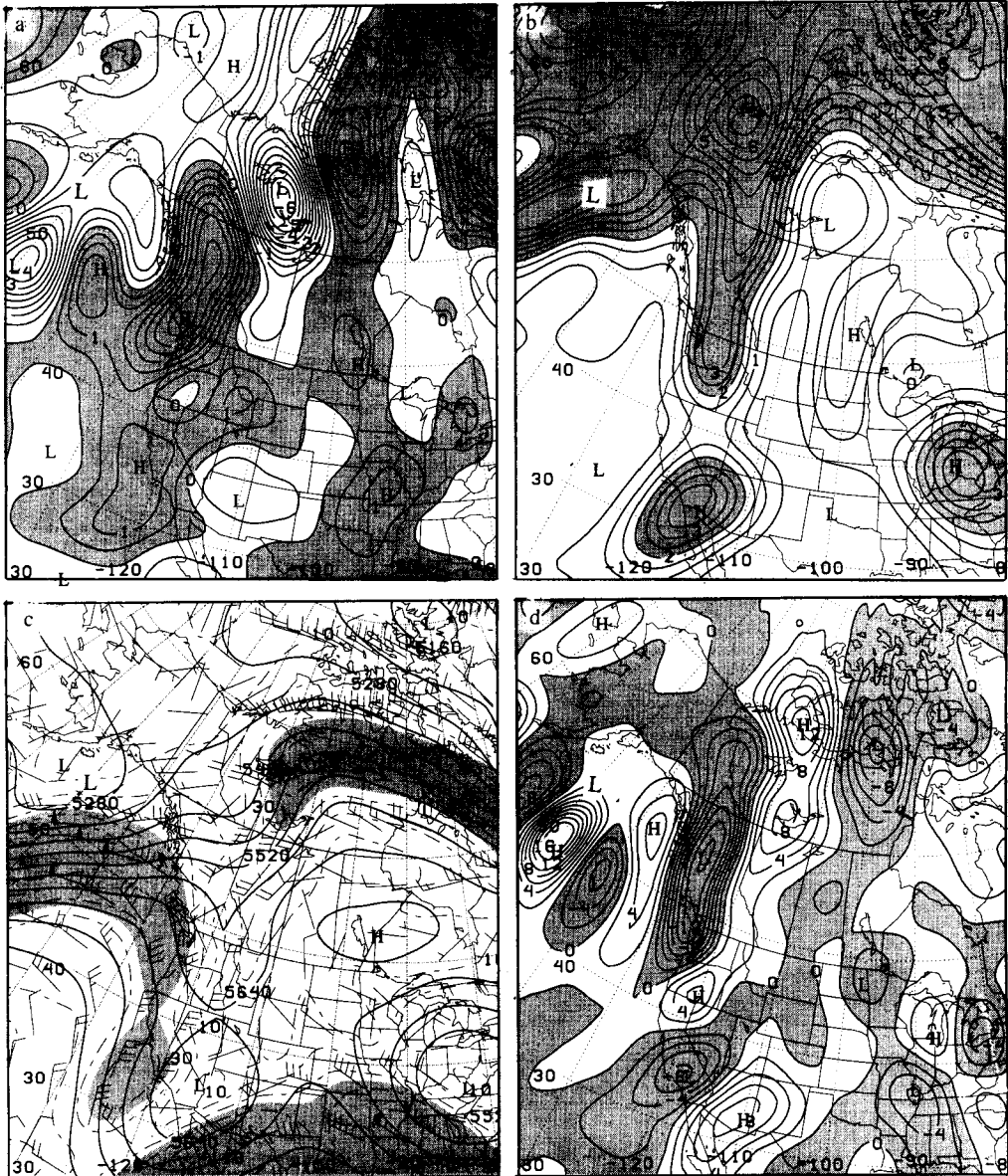


Figure 14. Horizontal distributions of (a) 500 hPa calculated ZO height tendency ( $\text{m s}^{-1}$ ), (b) 300 hPa Ertel potential vorticity (PVU), (c) 500 hPa heights (m) and 300 hPa winds ( $\text{m s}^{-1}$ ), and (d) 300 hPa PV advection ( $\text{PVU s}^{-1}$ ) ( $1 \times 10^{-11} \text{ PVU s}^{-1}$ ) for 0000 GMT 30 April 1980. The contour intervals are (a)  $5.0 \times 10^{-4} \text{ (m s}^{-1}\text{)}$ , (b) 0.5 PVU, (c) 60 m and  $10 \text{ (m s}^{-1}\text{)}$ , and (d) 2.0 ( $\text{PVU s}^{-1}$ ). Values greater than (a) 0, (b) 2.0, (c)  $35 \text{ (m s}^{-1}\text{)}$ , and (d) 0 are shaded in each. The wind barbs in (c) are the same as in Fig. 10.

south-west North America during development (see Fig. 13(c)). This perturbation then moved eastwards after 0000 GMT 24 April and bifurcated, with one piece continuing to move eastwards and the other becoming the perturbation in Fig. 15(b). After this time the perturbation deteriorated, and there was no further influx of low-PV air until after 0000 GMT 30 April.

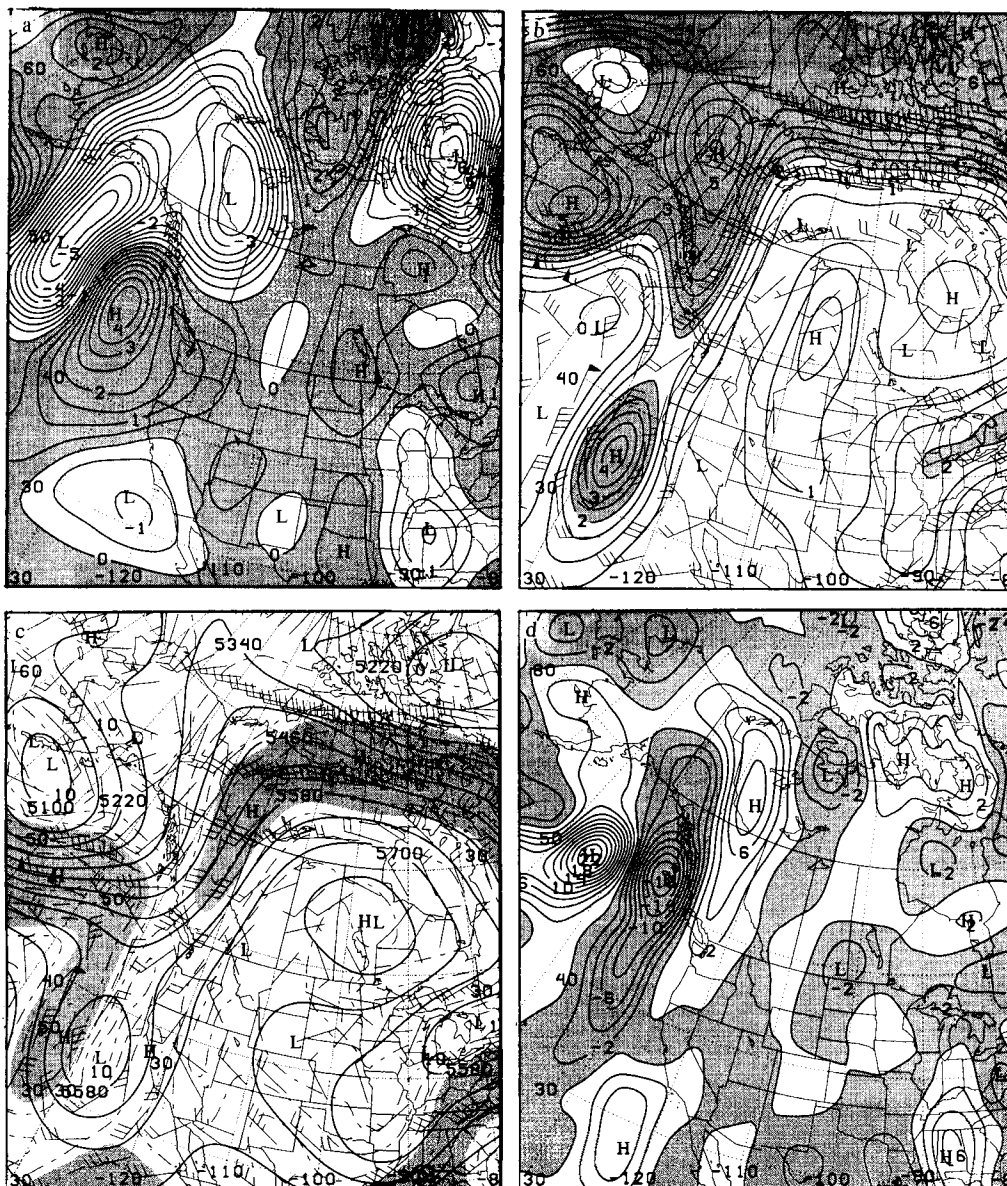


Figure 15. As in Fig. 14 except for 0000 GMT 27 April 1980.

(c) *Decay*

The time period chosen to represent decay begins at 0000 GMT 3 May 1980. The decay period was characterized by the block losing its intensity (Fig. 9) and identity (Fig. 16(c)) until the block no longer met the LS95a criteria after 0000 GMT 4 May. Also, a surface low (Fig. 16(c)), located on the north-west flank of the block over western Canada, was present at this time. Such a feature was also noted during the decay of the LS95b case and in one of the cases in Lupo (1997). Figure 16(a) demonstrates that height falls predominated over much of western Canada (in the blocking ridge), in association with the upper-air trough located on the north-west flank of the decaying block. The EPV distribution (Figs. 16(b)

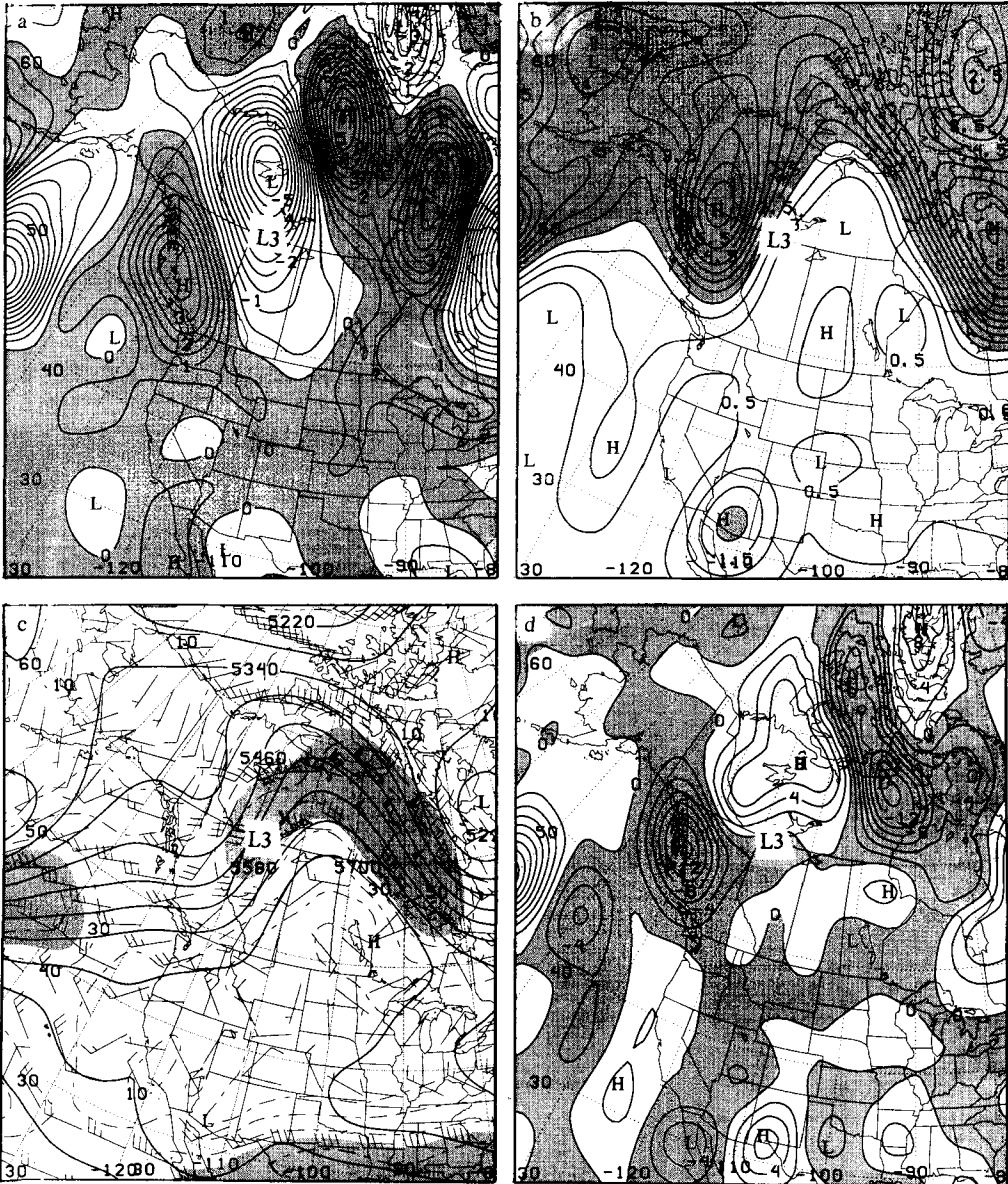


Figure 16. As in Fig. 14 except for 0000 GMT 3 May 1980. The surface low is marked with an 'L3'.

and (d) shows a corresponding region of high-PV air that impinged on the north-west flank of the block. This region of high-PV air did not penetrate very far equatorwards into the mid-latitudes and eventually fracture, as did similar regions of high-EPV air during formation and intensification periods (contrast with Figs. 11(c), 13(c) and 16(b)). However, this region of high-PV air does eventually break cyclonically (Thorncroft *et al.* 1993), and lack of penetration into the mid-latitudes is one of the features distinguishing the behaviour of such an event. There was also a region of higher-potential-vorticity air (1.0+ PVU) located within the ridge and over mid-North America. Inspection of the PV

evolution suggests that this high-PV perturbation 'broke off' from the main PV reservoir located polewards and then settled into the High Plains region.

(d) *Discussion*

In the previous section, it was shown that the planetary-scale flow regime contributed to the formation of this blocking anticyclone, at least partially, through the establishment of a favourable environment manifested by the presence of a planetary-scale quasi-stationary ridge. The block formation model of Tsou and Smith (1990) demonstrates the importance of such a feature prior to block onset. LS95a also noted that their model adequately described all blocking events in their sample. Even though blocking events can be described primarily by the planetary-scale components of the height field (e.g. Fournier 1996), planetary-scale dynamics and forcing alone clearly cannot account for the development and/or presence of blocking events in the northern hemisphere. Observations alone tells us that, despite the prominence of wave numbers 1, 2, and 3 in association with blocking, rarely is more than one blocking event observed at any one time over the entire northern hemisphere (Lejenas and Okland 1983; LS95a).

Others (e.g. Kalnay-Rivas and Merkinė 1981; Fredriksen 1982, 1983; Shutts 1983) first showed the maintenance of model blocking events by synoptic-scale transients. Using a simple model with a *wave maker* and no topography, Shutts (1983) showed in his *non-linear experiment* that a block develops only downstream of the *wave maker* even though the basic state was zonal, and the initial wind field can be described as wave number 3. The planetary-scale analyses of our blocking event showed that despite the presence of wave numbers 2 and 3 in the planetary-scale height field (Fig. 3), only one block developed. There are other similarities between this observed event and Shutts's modelling study. The blocking event studied here had a half-wavelength of about 3500 km, and the interacting cyclones (L1 and L2; see Fig. 10) were located about 40° to 60° longitude upstream of the event during block formation. These results are consistent with typical blocking events found in LS95a and Konrad and Colucci (1988) (with respect to the location of upstream cyclones). Thus, these cyclones were located roughly 3500 km (at latitudes of 45° to 60°) upstream of the block, which represents about one-half the large-scale wavelength (Table 1). This distance is consistent with the dimensions of the Shutts model block (~3000 km). Additionally, Shutts (1983) comments in his conclusions that as the wave maker moved upstream in his 'channel', so too did the block. Therefore, the evidence strongly suggests that not only are the synoptic-scale transients important to block formation, but also that the phase relationship of these transients to the planetary-scale features is important.

Figure 17 displays the entire subset of the surface cyclone tracks (connected dots) that occurred over the North Pacific region between 19 April and 4 May 1980. The cyclone tracks are numbered in parenthesis and the genesis time is noted beneath that number. The circled cross over south-east Saskatchewan represents the position of the block at *onset*. Several cyclones occurred upstream of the block throughout development and during its subsequent evolution. L1 (track (2) 12/19) and L2 (track (4) 00/23) were two of those cyclones. As stated above, L1 and L2 underwent a period of most rapid cyclogenesis about one-half wavelength upstream of the block and were, therefore, in an ideal position to be associated with block development as described previously. The surface cyclone that followed L2, track (3) 12/22, also developed rapidly within 60° longitude upstream of the block centre and was associated with block intensification after onset (see section 4(a) and refer to Figs. 9, 12 and 13). The only other cyclone in this set that was associated with block intensification (after 0000 GMT 30 April) is track (6) 00/27. This cyclone (Fig. 14) was at the end of a period of most rapid development when it moved within 60° longitude

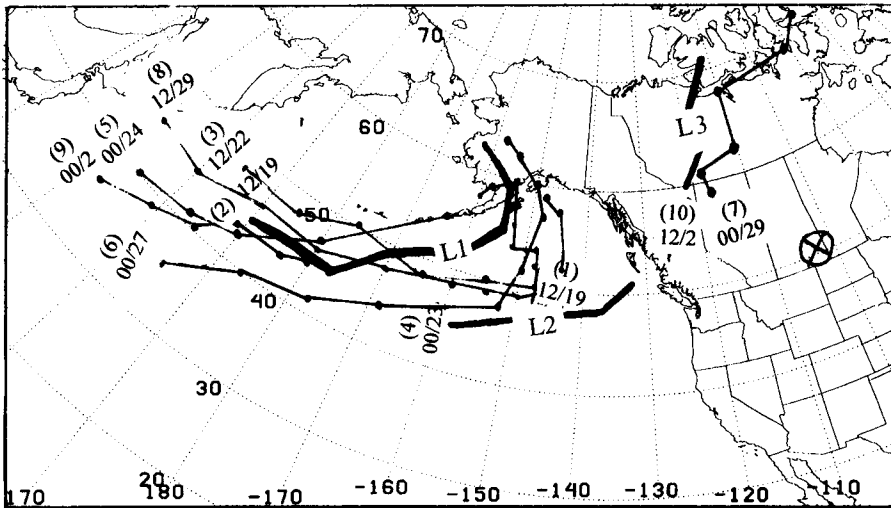


Figure 17. A map of all surface cyclone tracks (connected dots) occurring over the Pacific and North America region from 19 April through 4 May 1980. Each track is numbered in parenthesis at the genesis point and the genesis time is also noted. L1, L2, and L3, the heavier tracks, are surface lows highlighted in the text.

upstream of the block centre after 0000 GMT 29 April. All other cyclones in the set (e.g. track (5) 00/24, see section 4(b) discussion) apparently developed too far upstream and were not associated with development or intensification.

To support the importance of this phase relationship of the transients to block formation and maintenance, we contrast the relationship of an upstream cyclone, track (10) 12/2 marked with an L, and the block that occurred during the decay period (Figs. 16 and 17). LS95b and Lupo (1997) also noted the presence of an upstream cyclone during block decay in their case-studies. In all three cases, the surface cyclone was located much closer (within about  $15^\circ$  longitude, roughly 700 to 1000 km) to the block centre. Also, in all three cases the strong jet streaks were located at the apex (see Fig. 16(c) for this case) or on the downstream flank of the block. Thus, the associated upper-tropospheric advection of anticyclonic vorticity (not shown) was located downstream (north-east and east) of the block centre, and the block was not reinforced with the deposit of anticyclonic vorticity (Figs. 16(a) and (b)). This  $180^\circ$  phase relationship between the transients and the block seems crucial to the extent that the associated upper-air forcing favourable to cyclogenesis (anticyclogenesis) is located away from (within) the block region. Finally, it should also be mentioned here that in this case, the forcing favouring anticyclogenesis (upper-tropospheric anticyclonic-vorticity advection) was located in quadrature (approximately one-quarter wavelength) with the block on the upstream flank, a result in agreement with other blocking studies (e.g. Mullen 1987).

The results of this study suggest that, despite the anomalous planetary-scale flow regime that persisted through April 1980, the synoptic-scale formation and maintenance of this blocking event via cyclone-scale transients was similar to that of the cases studied by Tsou and Smith (1990), LS95a, and others. This study also shows that the Tsou and Smith (1990) block-formation paradigm can be explained using PV diagnostics. The results obtained by this study can be used in attempting to determine whether or not blocking anticyclones will intensify, be maintained, or weaken in regions where they are common; providing supplementary information to the model guidance. For example, it has been found by previous studies (Tsou and Smith 1990; LS95b; Lupo 1997) that blocking

anticyclones intensify, or at least are maintained, with the occurrence of upstream cyclones and the presence of jet maxima on the upstream flank of the block. These results suggest that this scenario is analogous to the 'digging' jet located in the upstream flank of deepening 500 hPa troughs. However, while being an aid in determining whether a block will intensify or decay, it would still be difficult to use the results of this study, and the others in this series, to forecast the development of blocking events since the 'blocking problem' is far from solved.

## 5. SUMMARY AND CONCLUSION

The planetary- and synoptic-scale forcing that contributed to the formation of a blocking anticyclone over the North American continent was examined in this paper. This event occurred in late April and early May of 1980, or immediately prior to the disastrous summer drought over central and south-eastern North America in that year. While the characteristics of the blocking event were typical for a spring season block occurring over a continental region as defined by LS95a, the presence of the block over North America was atypical as shown by previously published blocking climatologies, including LS95a. Using simple diagnostic techniques and the NMC analyses archived on CD-ROM, planetary-scale aspects of this event were examined to investigate the pre-block environment and determine to what extent this block could be considered anomalous. Synoptic-scale aspects of this blocking event were studied using the NCEP reanalyses and both the ZO equation and the PV approach, resulting in a complementary diagnosis.

The planetary-scale analysis of the pre-block and blocking environment showed that the flow over the Pacific and North America regions was anomalous in the sense that the regular (spring season) trough/ridge features over these regions were amplified, of shorter wavelength, and/or located further eastwards than are typical. This suggests that the anomalous flow regime that persisted during the spring season was primarily responsible for the anomalous occurrence of a blocking anticyclone over North America. This flow regime was, however, typical of the spring season during 1980, and the preceding winter (Namias 1982; Hoskins *et al.* 1983). The height field over North America resembled a typical summer pattern (e.g. Namias 1982), with a ridge over the continent and troughs along the east and west coasts. The corresponding positive height anomalies found over North America could then be associated with cooler than normal SSTs and the negative height anomalies over the central North Pacific. The combination of the North Pacific negative height anomalies and the positive height anomalies over the tropical Pacific (presumably linked to warmer SSTs there) and North America resulted in a stronger Pacific jet that was spread out across the entire ocean basin and into North America. At 850 hPa, anomalously high temperatures appeared over North America around mid-April and persisted throughout the block lifetime. In the absence of compensating upper-tropospheric cooling, this lower-tropospheric warming would contribute to ridging at 500 hPa over North America. This suggests that, at least in the time-mean sense, the lower-tropospheric processes can also contribute to block formation and maintenance. A simple Sutcliffe and 850 hPa thermodynamic analysis during the period prior to block formation demonstrated that 850 hPa temperature advection and subsidence associated with the advection of anticyclonic vorticity by the mean thermal wind were primarily responsible for the anomalous warmth at 850 hPa.

An examination of the synoptic-scale forcing showed that, in general, the block was formed and maintained in association with upstream surface cyclones. The synoptic aspects of the block-formation period were remarkably similar to those of the Tsou and Smith (1990) block, and the Tsou and Smith (1990) mechanisms were described using the

PV diagnostic framework. However, in this case, it was revealed that two cyclones could be identified in association with block formation. The question of whether one or more cyclones were involved in block formation as shown by Tsou and Smith (1990), LS95b, versus here, for example, may be more a matter of subjectivity in defining the 'development' period rather than of any dynamical significance, since this study endeavoured to examine individual cyclone interactions. The results of this study, and those of Lupo (1997) and Lupo and Smith (1998), suggest that blocking anticyclones fluctuate in intensity, as defined by LS95a, in association with upstream surface cyclone development. The same conclusion could be reached by using either the PV approach, or the ZO methodology. Many other studies have shown similar results, i.e. that blocks are formed and maintained by an ensemble of cyclone-scale transients (Frederiksen, personal communication) either observationally (i.e. Illari 1984; Mullen 1987) or using a variety of models (i.e. Shutts 1983; Mullen 1986). However, this study, like those of Konrad and Colucci (1988) or LS95b, focuses on interactions between particular cyclone events and block development.

The PV approach showed that the poleward sweep of low-EPV air, which was subsequently advected into the block region, was associated with both block formation and intensification. The low-PV air could be associated with higher pressure and warmer  $\theta$  on the tropopause, and was located along the anticyclonic-shear side of jet maxima found on the upstream flank of the developing block. Also, it was noted that during development and intensification, the upstream regions of high-PV air protruded deeper into the mid-latitudes and eventually 'fractured' from (anticyclonic breaking) the main PV reservoir as can commonly be associated with blocking (Thorncroft *et al.* 1993). During decay, the upstream high-PV air associated with the surface cyclone did not drive very far equatorwards, and eventually broke cyclonically (a more zonally elongated disturbance) as described by Thorncroft *et al.* (1993). Further study could reveal if this is a common occurrence during block decay. The ZO approach showed that the advection of anticyclonic vorticity was primarily responsible for strong height rises found over the developing block region. As in LS95a and Lupo and Smith (1998), these height rises were located on the anticyclonic-shear side on the upstream jet maximum. Additionally, the 500 hPa height tendencies correlated negatively with 300 hPa PV advection (significant at the 95% level), and it is suggested that 500 hPa ZO height rises and the advection of low-PV air at 300 hPa on the upstream flank of the block are both signatures that can be associated with block development and/or intensification. Finally, the synoptic-scale analysis suggests that despite the anomalous occurrence of this block over North America during the spring season, and the anomalous planetary-scale flow regime that accompanied it, this block was formed in a similar manner to other northern hemisphere blocking events.

This blocking event had characteristics in common with the simple model results of Shutts (1983). Both studies confirm the important role played by synoptic-scale transients, even though studies have shown that the planetary-scale components of the 500 hPa height field principally describe a blocking event. In particular, it was shown in this study, that despite the wave number 2 and 3 character of the planetary-scale flow, only one block formed in the northern hemisphere. A similar result was shown in the Shutts model study, as one block formed downstream of a 'wave maker'. This diagnosis shows that, typically, the interacting upstream cyclones develop most rapidly about one-half wavelength upstream of the blocking anticyclone. This is consistent with the climatological results of LS95a, and the Shutts model study. This suggests that the proper phase relationship between the synoptic-scale cyclones and the planetary-scale ridge (about one half-wavelength) is necessary for the amplification of the 500 hPa short-wave ridge and its subsequent 'phase locking' with the planetary-scale ridge. Finally, this phase relationship is also necessary for the favourable location of the advection of anticyclonic vorticity, or low-PV air into

the blocking region, thus providing the continuous reinforcement of anticyclonic vorticity necessary to maintain the block.

#### ACKNOWLEDGEMENTS

We would like to thank Eric Hoffman and Dr Ernest C. Kung for their helpful comments on this manuscript and discussion of the results. We would also like to thank John McBride and the anonymous reviewer whose comments were very helpful in strengthening the presentation of the results. This research was supported by the National Science Foundation through grant number ATM-9413012, which was awarded to the State University of New York at Albany.

#### REFERENCES

- Alberta, T. L., Colucci, S. J. and Davenport, J. C. 1991 Rapid 500mb cyclogenesis and anticyclogenesis. *Mon. Weather Rev.*, **119**, 1186–1204
- Austin, J. F. 1980 The blocking of middle latitude westerly winds by planetary waves. *Q. J. R. Meteorol. Soc.*, **106**, 327–350
- Blackmon, M. L., Wallace, J. M., Lau, N.-C. and Mullen, S. L. 1977 An observational study of the Northern Hemisphere winter circulation. *J. Atmos. Sci.*, **34**, 1040–1053
- Blackmon, M. L., Lee, Y.-H. and Wallace, J. M. 1984 Horizontal structure of 500mb height fluctuations with long, intermediate, and short time scales. *J. Atmos. Sci.*, **41**, 961–979
- Bosart, L. F. and Lackmann, G. M. 1995 Postlandfall tropical cyclone reintensification in a weakly barotropic environment: A case study of Hurricane David (September 1979). *Mon. Weather Rev.*, **123**, 3268–3291
- Charney, J. G. and DeVore, J. G. 1979 Multiple flow equilibria in the atmosphere and blocking. *J. Atmos. Sci.*, **36**, 1205–1216
- Colucci, S. J. 1985 Explosive cyclogenesis and large-scale circulation changes: Implications for atmospheric blocking. *J. Atmos. Sci.*, **42**, 2701–2717
- 1987 Comparative diagnosis of blocking versus non-blocking planetary circulation changes during synoptic-scale cyclogenesis. *J. Atmos. Sci.*, **44**, 124–139
- Colucci, S. J. and Baumhefner, D. P. 1998 Numerical prediction of the onset of blocking: A case study with forecast ensembles. *Mon. Weather Rev.*, **126**, 773–784
- Colucci, S. J., Loesch, A. Z. and Bosart, L. F. 1981 Spectral evolution of a blocking episode and comparison with wave interaction theory. *J. Atmos. Sci.*, **38**, 2092–2111
- Dickson, R. R. 1980 Weather and circulation of June, 1980—Inception of a heat wave and drought over the central and southern Great Plains. *Mon. Weather Rev.*, **108**, 1469–1474
- Dole, R. M. 1986 The life cycles of persistent anomalies and blocking over the North Pacific. *Adv. Geophys.*, **29**, 31–70
- Ertel, H. 1942 Ein neuer hydrodynamischer Wirbesatz. *Meteorol. Z.*, **59**, 277–281
- Frederiksen, J. S. 1982 A unified three-dimensional instability theory of the onset of blocking and cyclogenesis. *J. Atmos. Sci.*, **39**, 969–982
- 1983 A unified three-dimensional instability theory of the onset of blocking and cyclogenesis II. Teleconnection patterns. *J. Atmos. Sci.*, **40**, 2593–2609
- Fournier, A. 1996 ‘Wavelet analysis of observed geopotential and wind: blocking and local energy coupling across scales’. *Wavelet applications in signal and image processing IV*. SPIE Proceedings Vol. 2825
- Haltiner, G. J. and Williams, R. T. 1980 *Numerical prediction and dynamic meteorology*. John Wiley and Sons, New York
- Holton, J. R. 1979 *An introduction to dynamic meteorology, 2nd ed.* Academic Press Inc., New York
- Hoskins, B. J. and Berrisford, P. 1988 A potential vorticity perspective of the storm of 15–16 October 1987. *Weather*, **43**, 122–129
- Hoskins, B. J., James, I. N. and White, G. H. 1983 The shape, propagation, and mean-flow interaction of large-scale weather systems. *J. Atmos. Sci.*, **40**, 1595–1612
- Hoskins, B. J., McIntyre, M. E. and Robertson, A. W. 1985 On the use and significance of isentropic potential vorticity maps. *Q. J. R. Meteorol. Soc.*, **111**, 877–946

- Hurrell, J. W. 1996 Influence of variations in extratropical wintertime teleconnections on Northern Hemisphere temperatures. *Geophys. Res. Lett.*, **23**, 665–668
- Illari, L. 1984 A diagnostic study of the potential vorticity in a warm blocking anticyclone. *J. Atmos. Sci.*, **41**, 3518–3525
- Kalnay-Rivas, E. and Merkinė, L. O. 1981 A simple mechanism for blocking. *J. Atmos. Sci.*, **38**, 2077–2091
- Kalnay, E., Kanamitsu, M., Kisler, R., Collins, W., Deaven, D., Gandin, L., Iredell, M., Saha, S., White, G., Woolen, J., Zhu, Y., Chelliah, M., Ebisuzaki, W., Higgins, W., Janowiak, J., Mo, K. C., Ropelowski, C., Wang, J., Leetmaa, A., Reynolds, R., Jenne, R. and Joseph, D. 1996 The NCEP/NCAR 40-year reanalysis project. *Bull. Am. Meteorol. Soc.*, **77**, 437–471
- Konrad, C. E. and Colucci, S. J. 1988 Synoptic climatology of 500 mb circulation changes during explosive cyclogenesis. *Mon. Weather Rev.*, **116**, 1431–1443
- Kung, E. C., Susskind, J. and Dacamera, C. C. 1993 Prominent Northern Hemisphere winter blocking episodes and associated anomaly fields of sea surface temperatures. *Terr. Atmos. Ocean Sci.*, **4**, 273–291
- Lejenas, H. and Madden, R. A. 1992 Travelling planetary-scale waves and blocking. *Mon. Weather Rev.*, **120**, 2821–2830
- Lejenas, H. and Okland, H. 1983 Characteristics of Northern Hemisphere blocking as determined from a long time series of observational data. *Tellus*, **35A**, 350–362
- Livezey, R. E. 1980 Weather and circulation of July, 1980—Climax of historic heat wave and drought over the United States. *Mon. Weather Rev.*, **108**, 1708–1716
- Lupo, A. R. 1997 A diagnosis of two blocking events that occurred simultaneously over the mid-latitude Northern Hemisphere. *Mon. Weather Rev.*, **125**, 1801–1823
- Lupo, A. R. and Smith, P. J. 1995a Climatological features of blocking anticyclones in the Northern Hemisphere. *Tellus*, **47A**, 439–456
- 1995b Planetary and synoptic-scale interactions during the life cycle of a mid-latitude blocking anticyclone over the North Atlantic. *Tellus*, **47A**, 575–596
- 1998 The interactions between a mid-latitude blocking anticyclone and a synoptic-scale cyclone occurring in the summer season. *Mon. Weather Rev.*, **126**, 503–515
- Lupo, A. R., Smith, P. J. and Zwack, P. 1992 A diagnosis of the explosive development of two extratropical cyclones. *Mon. Weather Rev.*, **120**, 1490–1523
- McIntyre, M. 1988 ‘The dynamical significance of isentropic distributions of potential vorticity and low-level distributions of potential temperature’. Pp. 237–259 in Vol. 1, Proceedings of the nature and prediction of extratropical weather systems. European Centre for Medium-Range Weather Forecasts, Reading, UK
- McWilliams, J. C. 1980 An application of equivalent modons to atmospheric blocking. *Dyn. Atmos. Ocean*, **5**, 43–46
- Mak, M. 1991 Dynamics of an atmospheric blocking as deduced from its local energetics. *Q. J. R. Meteorol. Soc.*, **117**, 477–493
- Mass, C. F., Edmon, E. J., Friedman, H. J., Cheney, N. R. and Recker, E. E. 1987 The use of compact discs for the storage of large meteorological and oceanographic data sets. *Bull. Am. Meteorol. Soc.*, **68**, 1556–1558
- Mo, K. C. and Livezey, R. E. 1986 Tropical–extratropical geopotential height teleconnections during the Northern Hemisphere winter. *Mon. Weather Rev.*, **114**, 2488–2515
- Mullen, S. L. 1986 The local balances of vorticity and heat for blocking anticyclones in a spectral general circulation model. *J. Atmos. Sci.*, **43**, 1406–1441
- 1987 Transient eddy forcing and blocking flows. *J. Atmos. Sci.*, **44**, 3–22
- Nakamura, H., Lin, G. and Yamagata, T. 1997 Decadal climate variability in the Northern Pacific during recent decades. *Bull. Am. Meteorol. Soc.*, **78**, 2215–2226

- Namias, J. 1982 Anatomy of great plains protracted heat waves (especially the 1980 U.S. summer drought). *Mon. Weather Rev.*, **110**, 824–838
- 1983 Some causes of the United States drought. *J. Clim. Appl. Meteorol.*, **22**, 30–39
- Neter, J., Wasserman, W. and Whitmore, G. A. 1988 *Applied statistics*, 3rd Edition. Allyn and Bacon Press, Boston, MA
- Nielsen-Gammon, J. W. and Lefevre, R. J. 1996 Piecewise tendency diagnosis of dynamical processes governing the development of an upper-tropospheric trough. *J. Atmos. Sci.*, **53**, 3120–3142
- Pedlosky, J. 1987 *Geophysical fluid dynamics*, 2nd ed. Springer-Verlag, Berlin
- Pettersen, S. 1956 *Weather analysis and forecasting*. Vol. I., 2nd ed. McGraw-Hill
- Quiroz, R. S. 1987 Travelling waves and regional transitions in blocking activity in the Northern Hemisphere. *Mon. Weather Rev.*, **115**, 919–935
- Rex, D. F. 1950 Blocking action in the middle troposphere and its effect on regional climate II. The climatology of blocking action. *Tellus*, **2**, 275–301
- Shukla, J. and Mo, K. C. 1983 Seasonal and geographical variation of blocking. *Mon. Weather Rev.*, **111**, 388–402
- Shutts, G. J. 1983 The propagation of eddies in diffluent jet streams: Eddy vorticity forcing of blocking flow fields. *Q. J. R. Meteorol. Soc.*, **109**, 737–761
- 1986 A case study of eddy forcing during an Atlantic blocking episode. *Adv. Geophys.*, **29**, 135–161
- Simmons, A. J. 1986 Numerical prediction: some results from operational forecasting at ECMWF. *Adv. Geophys.*, **29**, 305–338
- Simmons, A. J., Branstator, G. W. and Wallace, J. M. 1983 Barotropic wave propagation and instability and atmospheric teleconnection patterns. *J. Atmos. Sci.*, **40**, 729–743
- Sinclair, M. R. 1996 A climatology of anticyclones and blocking for the Southern Hemisphere. *Mon. Weather Rev.*, **124**, 245–263
- Sperenza, A. 1986 Deterministic and statistical properties of Northern Hemisphere middle latitude circulation. *Adv. Geophys.*, **29**, 226
- Thorncroft, C. D., Hoskins, B. J. and McIntyre, M. E. 1993 Two paradigms of baroclinic wave life-cycle behavior. *Q. J. R. Meteorol. Soc.*, **119**, 17–56
- Tibaldi, S. and Molteni, F. 1990 On the operational predictability of blocking. *Tellus*, **42A**, 343–365
- Tibaldi, S., Ruti, P., Tosi, E. and Maruca, M. 1993 ‘Operational predictability of winter blocking: An ECMWF update’. Proceedings of ECMWF seminars on validation of forecasts and large-scale simulations over Europe. European Centre for Medium-Range Weather Forecasts, Reading, UK
- Tibaldi, S., Tosi, E., Navarra, A. and Pedulli, L. 1994 Northern and Southern Hemisphere seasonal variability of blocking frequency and predictability. *Mon. Weather Rev.*, **122**, 1971–2003
- Tracton, M. S. 1990 Predictability and its relationship to scale interaction processes in blocking. *Mon. Weather Rev.*, **118**, 1666–1695
- Trenberth, K. E. and Mo, K. C. 1985 Blocking in the Southern Hemisphere. *Mon. Weather Rev.*, **113**, 3–21
- Triedl, R. A., Birch, E. C. and Sajecki, P. 1981 Blocking action in the Northern Hemisphere. A climatological study. *Atmos.-Ocean*, **19**, 1–23
- Tsou, C. H. and Smith, P. J. 1990 The role of synoptic/planetary-scale interactions during the development of a blocking anticyclone. *Tellus*, **42A**, 174–193
- Tung, K. K. and Lindzen, R. S. 1979a A theory of stationary long waves, part I: A simple theory of blocking. *Mon. Weather Rev.*, **107**, 714–734
- 1979b A theory of stationary long waves, part II: Resonant Rossby waves in the presence of realistic vertical shear. *Mon. Weather Rev.*, **107**, 735–750
- Wagner, A. J. 1980 Weather and circulation of August, 1980—Eastward spread of heat wave and drought. *Mon. Weather Rev.*, **108**, 1924–1932
- Wallace, J. M. and Gutzler, D. S. 1981 Teleconnections in the geopotential height field during the Northern Hemisphere winter. *Mon. Weather Rev.*, **109**, 784–812
- Zwack, P. and Okossi, B. 1986 A new method for solving the quasi-geostrophic omega equation by incorporating surface pressure tendency data. *Mon. Weather Rev.*, **114**, 655–666